At the bottom, $z = 0$, we have $K = 0$, and at the surface $s = h$, we have

$$\eta \frac{\partial u}{\partial s} = \tau_x \text{ and } K(z, h) = \int_0^z \frac{ds}{\eta}.$$

Furthermore

$$\eta \frac{\partial K}{\partial s} = 0; s > z \text{ and } \eta \frac{\partial K}{\partial s} = 1; s < z.$$

The result of the integration is then

$$\tau_x \int_0^z \frac{ds}{\eta} - u.$$

In the equations we replace z by s and integrate between 0 and h, giving the equations

$$\int_0^h K(z, s) \left(- \varrho \lambda v + \frac{\partial p}{\partial x} \right) ds = \tau_x \int_0^z \frac{\partial s}{\eta} - u,$$

$$\int_0^h K(z, s) \left(\varrho \lambda u + \frac{\partial p}{\partial y} \right) ds = \tau_y \int_0^z \frac{ds}{\eta} - v.$$

We multiply these equations by dx and dy and integrate along a stream line:

$$\int_0^h K(z, s) \left[\int \varrho \lambda \, (u dy - v dx) + \int dp \right] ds = \int_0^z \frac{ds}{\eta} \left(\int \tau_x \, dx + \tau_y \, dy \right) - \int u dx + v dy.$$

Along the stream line

$$u dy - v dx = 0,$$

and if the integration contour is also closed, we have

$$\oint dp = 0.$$

$C = \oint (u dx + v dy)$ is the circulation along the closed stream line, and we get

$$C = \int_0^z \frac{ds}{\eta} \oint (\tau_x \, dx + \tau_y \, dy).$$

$\oint (\tau_x \, dx + \tau_y \, dy)$ is the work done by the tangential stress of the wind along the same stream line. We then get the result that under these assumptions the circulation is proportional to the work done by the wind.

(Manuscript received 6 December 1961)

At the bottom, $z = 0$, we have $K = 0$, and at the surface $s = h$, we have

$$\eta \frac{\partial u}{\partial s} = \tau_x \text{ and } K(z, h) = \int_0^z \frac{ds}{\eta}.$$

Furthermore

$$\eta \frac{\partial K}{\partial s} = 0; s > z \text{ and } \eta \frac{\partial K}{\partial s} = 1; s < z.$$

The result of the integration is then

$$\tau_x \int_0^z \frac{ds}{\eta} - u.$$

In the equations we replace z by s and integrate between 0 and h, giving the equations

$$\int_0^h K(z, s) \left(- \varrho \lambda v + \frac{\partial p}{\partial x} \right) ds = \tau_x \int_0^z \frac{\partial s}{\eta} - u,$$

$$\int_0^h K(z, s) \left(\varrho \lambda u + \frac{\partial p}{\partial y} \right) ds = \tau_y \int_0^z \frac{ds}{\eta} - v.$$

We multiply these equations by dx and dy and integrate along a stream line:

$$\int_0^h K(z, s) \left[\int \varrho \lambda \, (u dy - v dx) + \int dp \right] ds = \int_0^z \frac{ds}{\eta} \left(\int \tau_x \, dx + \tau_y \, dy \right) - \int u dx + v dy.$$

Along the stream line

$$u dy - v dx = 0,$$

and if the integration contour is also closed, we have

$$\oint dp = 0.$$

$C = \oint (u dx + v dy)$ is the circulation along the closed stream line, and we get

$$C = \int_0^z \frac{ds}{\eta} \oint (\tau_x \, dx + \tau_y \, dy).$$

$\oint (\tau_x \, dx + \tau_y \, dy)$ is the work done by the tangential stress of the wind along the same stream line. We then get the result that under these assumptions the circulation is proportional to the work done by the wind.

(Manuscript received 6 December 1961)

THE NORWEGIAN CYCLONE MODELS IN RELATION TO HEAT AND COLD SOURCES

BY

SVERRE PETTERSSEN,

DOROTHY L. BRADBURY and KAARE PEDERSEN

Department of the Geophysical Sciences
The University of Chicago

FREMLAGT I VIDENSKAPS-AKADEMIETS MØTE DEN 9DE FEBRUAR 1962

Summary. Typical cases of cyclone development on the North Atlantic have been analyzed; the eddy fluxes of latent and sensible heat, the radiative heat fluxes, and the dissipation of kinetic energy have been computed. The data are organized to supplement the classical cyclone models, including: nascent cyclone waves, warm-sector cyclones, partly occluded cyclones, full occlusions, cold-core frontless lows, and outbreaks of arctic air in the rear of major cyclones or families of cyclones. Comparison with a large number of cyclone developments in North America (to the east of the Continental Divide) showed remarkable differences: On the North Atlantic the initial development appears to be due mainly to thermal advection in the lower half of the troposphere, while on the North American continent the onset of development is normally brought about by a marked upper cold trough (with strong vorticity advection on its forward side) that approaches a low-level frontal zone.

The vorticity equation and the thermodynamic energy equation are used to obtain a diagnostic equation for the vertical velocity and a prognostic equation for the thickness of layers bounded by isobaric surfaces. The equations are used to obtain numerical estimates of the effects of heat and cold sources (sensible and released latent heat) on the rate of development. The data computations provide information on the conditions typical of nascent cyclone waves, warm-sector cyclones, partly occluded cyclones, and full occlusions. The results indicate that the heat and cold sources associated with eddy transfers of sensible heat from the ocean surface and with liberation of latent heat in the cloud systems contribute significantly to cyclone development. At such low temperatures as are typical of the North Atlantic region in winter, the energy sources normally rank in the following descending order: potential energy, eddy transfer from the ocean, and liberated latent heat. At such high temperatures and moistures as are typical of the intertropical belt, the effect of the liberated latent heat is likely to be a dominant one.

1. Introduction. *1.1. General.* The research that forms the basis of this paper[1] has resulted in the production of much data on the large-scale aspects of ocean-atmosphere interactions, particularly insofar as exchanges of heat and water vapor are concerned. The present paper, however, deals only with the effects of heat and cold sources on cyclone development. As far as possible, the results are presented in relation to the classical cyclone models developed more than forty years ago by VILHELM BJERKNES and his collaborators.

The region chosen for the synoptic analyses is the North Atlantic Ocean, and emphasis has been placed upon the western part of the region and on the cold season, so as to obtain cases with large thermal contrasts.

The data analyses involve evaluations of evaporation, eddy and radiative heat exchanges, and dissipation of kinetic energy at the ocean-atmosphere interface and within the atmosphere. The working formulae used are explained and referenced in the Appendix on p. 278 and the mathematical symbols are defined in List of Symbols on p. 279.

1.2. Choice of Cases. The synoptic situations were chosen so as to be typical representatives of the various stages of cyclone development, as represented by the aforementioned cyclone models, namely: the nascent cyclone wave, the warm-sector cyclone, the partly occluded cyclone, the full occlusion, and the frontless cold-core low. In addition certain characteristics of outbreaks of artic air masses were examined.

A number of pre-established criteria guided the choice of cases of cyclone developments. To qualify for inclusion in this study, each case had: (a) to be simple, in the sense that it should contain only a single frontal zone, be broadly of normal dimensions, and be well separated from neighboring cyclones; (b) to be well within the normal cyclone belt on the North Atlantic; (c) to be well covered by synoptic data; and (d) to be clearly identifiable as a major system for a period of at least 24 hours. In all, 51 individual cases of cyclone development were used.

In the case of outbreaks of artic air, the requirements were that each outbreak (a) should be rooted in an arctic air mass with its main body to the north of 65°N; (b) should make up the rear of a major cyclone of the occluded or cold-core type; (c) should have a distinct core with a maximum wind speed exceeding 15 m sec^{-1}; and, (d) should penetrate into the subtropical anticyclonic belt. With these criteria each outbreak covered only a limited east-west span, sometimes not more than 1000 km.

1.3. Construction of Cyclone Models. Since one of the purposes of the present investigation was to obtain realistic models of typical stages in the life history of cyclones, without distortions due to peculiarities of individual cases, a flexible grid system was introduced so that mean structures of similar cases could be obtained. The system of

[1] The research here referred to has been sponsored by the Geophysics Research Directorate of the Air Force Cambridge Research Laboratories, Air Research and Development Command, under Contract No. AF 19(604)—7230, and by the National Science Foundation under Grant 6385. The able assistance of Messrs. Ramesh V. Godbole, Gandikota V. Rao, and Gerald F. Watson, Jr. in the data processing is gratefully acknowledged.

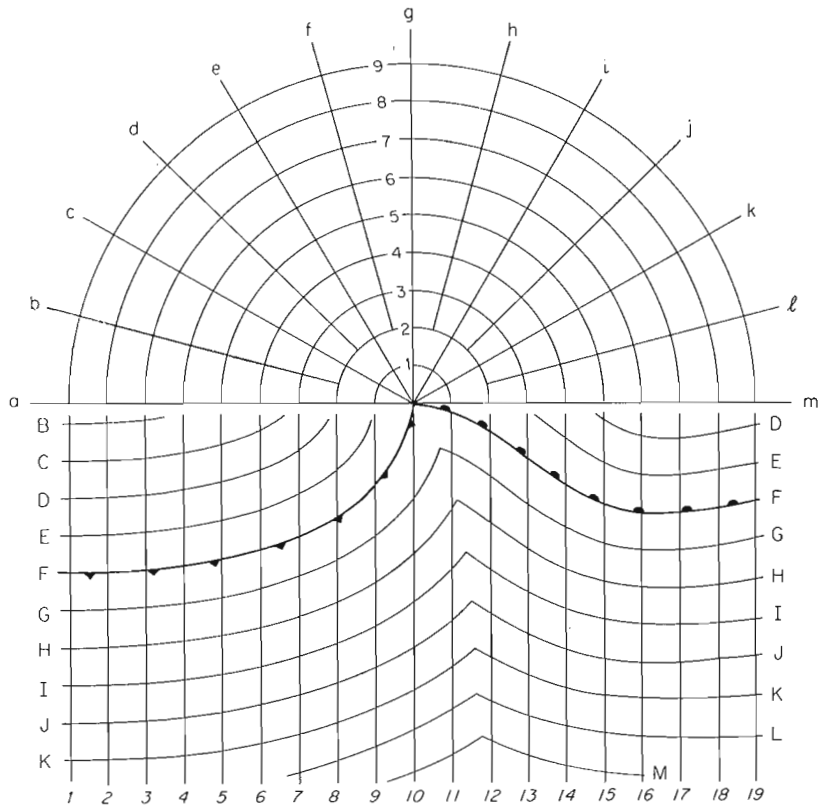

Fig. 1. System of grid points used in compiling data on warm-sector cyclones. Similar grids were used in connection with the other stages of development.

grid points was allowed to vary in detail from one principal stage of development to another, but the essential features are common for all, and these may be described with reference to Fig. 1 which applies to warm-sector cyclones. In each case equidistant lines E, F, G, etc. were drawn on the synoptic chart parallel to the front and 300 km apart. Another set of lines, f, g, h, etc., were drawn radially from the center of the cyclone (or from the apex of the wave), and a third set, 1, 2, 3, etc., indicated the distances shown. This system of coordinate lines provided grid points arranged in relation to the center and the frontal zone of the cyclone in question. In each case, the pressure, temperature, moisture, wind, and weather category (Fig. 2) were read at each grid point, and so were the computed values of the fluxes of sensible and latent heat, rate of dissipation, etc. Next, all data pertaining to the same stage of cyclone development were compounded into mean values for each grid point, and then transferred to a master grid of the type shown in Fig. 1. Finally, the mean state was obtained and represented by isopleths on the master grid. The end results (without the master grids) are shown in Fig. 3—7.

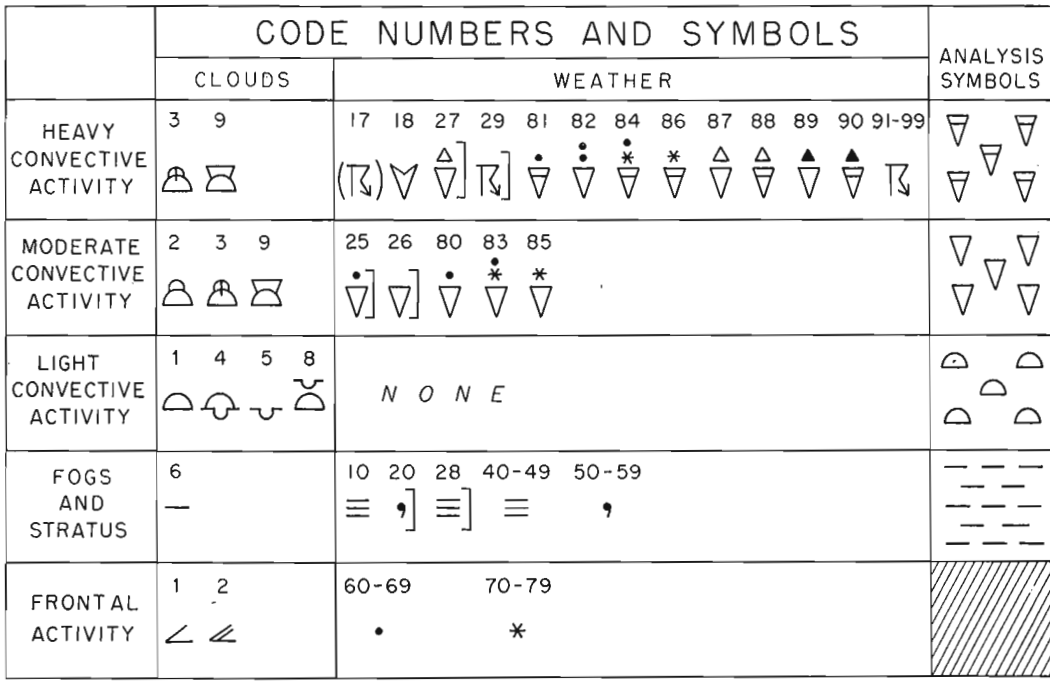

Fig. 2. Classification of cloud and weather regions.

With reference to Fig. 1 it should be noted that the line g—10 marks the meridian through the center, which is at the intersection of a—m and g—10. Thus by superimposing all similar cases, in such a manner that the lines a—m and g—10 coincide, fields representing mean (or model) development stages were obtained.

To determine the number of cases needed to obtain stable models the criterion was used that the mean isobars should be obtained without smoothing. In the models representing the stages of development of frontal cyclones 12 cases proved ample, and in the case of the cold-core low 6 cases sufficed.

The individual cyclones that went into each model showed some geographical scatter, particularly in the east—west direction, and to represent the sequence of models in a realistic manner each model was transferred to a customary base chart and centered at the mean position of the cases used, while retaining the orientation of the meridian. The sequence of models in Figs. 3—7 shows, therefore, an east-northeastward drift reflecting the normal behavior of developing cyclones on the North Atlantic.

1.4. Classification of Weather Regions. In order to depict the simultaneous developments of weather and motion systems, it was necessary to incorporate in the pictorial models fields of clouds and weather based upon some broad classification. In concert with current nomenclature, the observed weather (clouds and precipitation) was referred to the following categories: *frontal*, *convective*, and *stable*. The convective weather

was subdivided into three classes, according to intensity, as shown in Fig. 2. Borders between each region were drawn on each synoptic chart and the class number noted at the intersections of the grids explained in Section 1.3. Thereafter, the frequencies of the class numbers were entered at the grid intersections in each of the composite models.

On the basis of these frequencies, the term *predominant weather* was defined as that class which accounted for more than 50 per cent of the total. In a few areas of limited extent no single class had a frequency of occurrence equal to or larger than 50 per cent. In such cases the two classes with the highest frequency of occurrence were joined to form a mixed type. To indicate the steadiness of the patterns, the percentage probability of occurrence of the predominant type is indicated in each case. Thus, for example, in Fig. 4 the probability of light convection (see Fig. 2) is close to 100 per cent over a large area to the south of the wave disturbance, while the probability of heavy convection is 55 per cent in the cold air in the rear of the cyclone.

2. Cyclone models. For convenience, the life history of the model cyclone will be presented in two series of charts, the first showing the sequence of events at sea level, and the second depicting the sequence of vertical structures. Throughout, it will be useful to bear in mind that the models apply to the winter season. During the cold part of the year loss of heat by the air to the ocean waters is a rare occurrence, while in summer such losses are more frequent and widespread.

2.1. Sequences at Sea Level. During the cold season the frequency of occurrence of nascent cyclone waves has a distinct maximum off the coast of the United States. When the cold front is close to the coast the heat flux into the cold air could not be computed; for this reason use had to be made either of waves which formed to the east of the preferred cyclogenetic area, or of slowly amplifying waves which had moved out from the coastal region. The mean position of the young waves used in this investigation (Chart A of Fig. 3) is, therefore, farther to the east than what would have been the case if an unbiased sample had been used. Furthermore, since only well-defined systems were chosen for inclusion in the study, the circulation, as indicated by the isobars, is rather stronger than that pertaining to a random sample.

Charts A in Figs. 3—7 show the sequence of pressure distributions and frontal structures at sea level. As one would expect, these conform in all essentials to the idealized models proposed 40 years ago by Bjerknes and collaborators. For the discussion that follows it is of some interest to note that the young wave (Fig. 3, Chart A) is generously supplied with tropical air with origin in the tradewind belt, which is considerably perturbed in tune with the wave disturbance.

Charts B in Figs. 3—7 show the rate of dissipation of kinetic energy at the ocean-atmosphere interface. The dissipation within the atmosphere was always very small and, for all practical purposes, Chart B may be taken to represent the total dissipation. Since the surface dissipation is proportional to the cube of the wind speed (not assumed

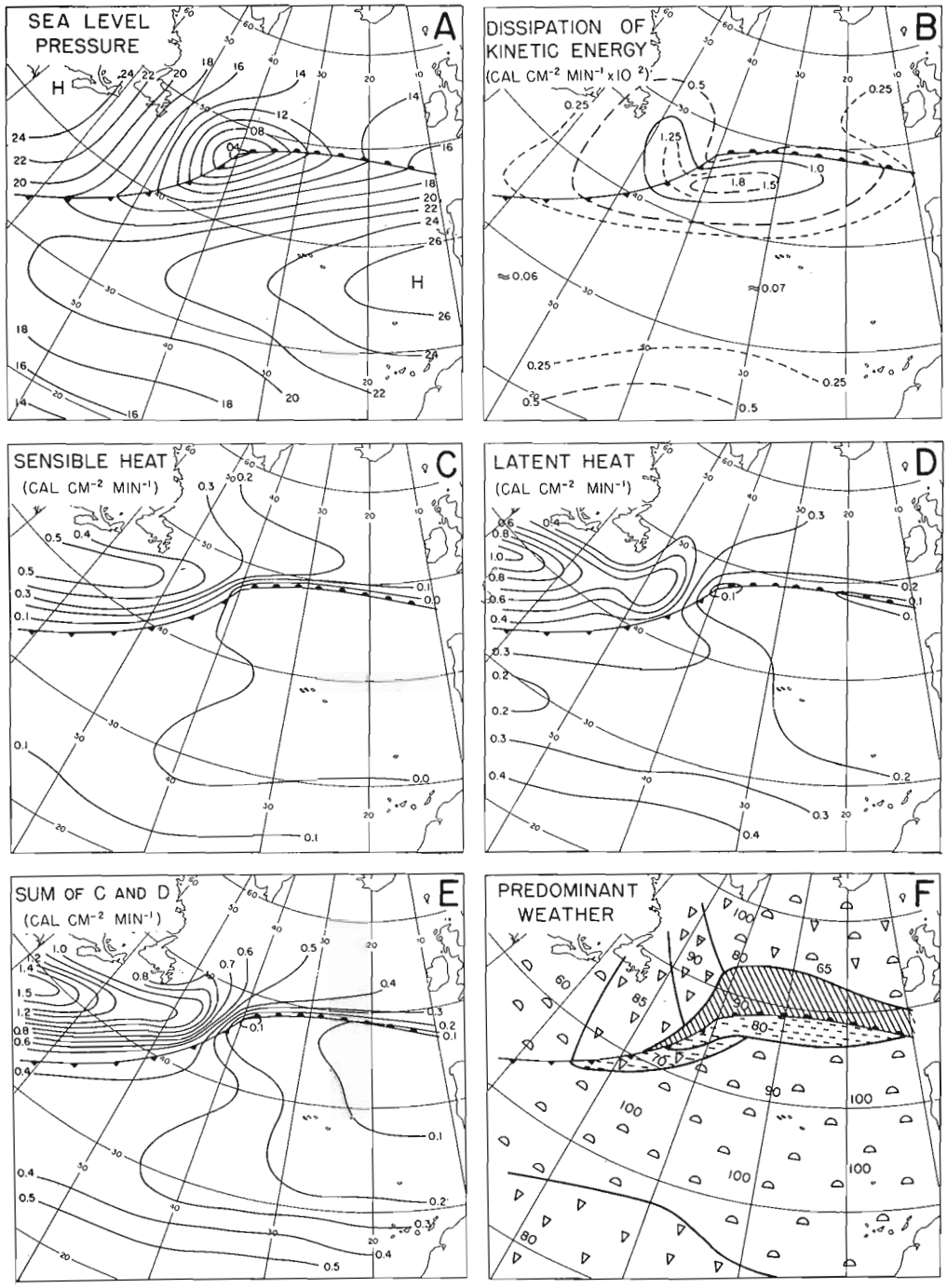

Fig. 3. Models of nascent cyclone waves. Note that the values in Chart B have been multiplied by 100.

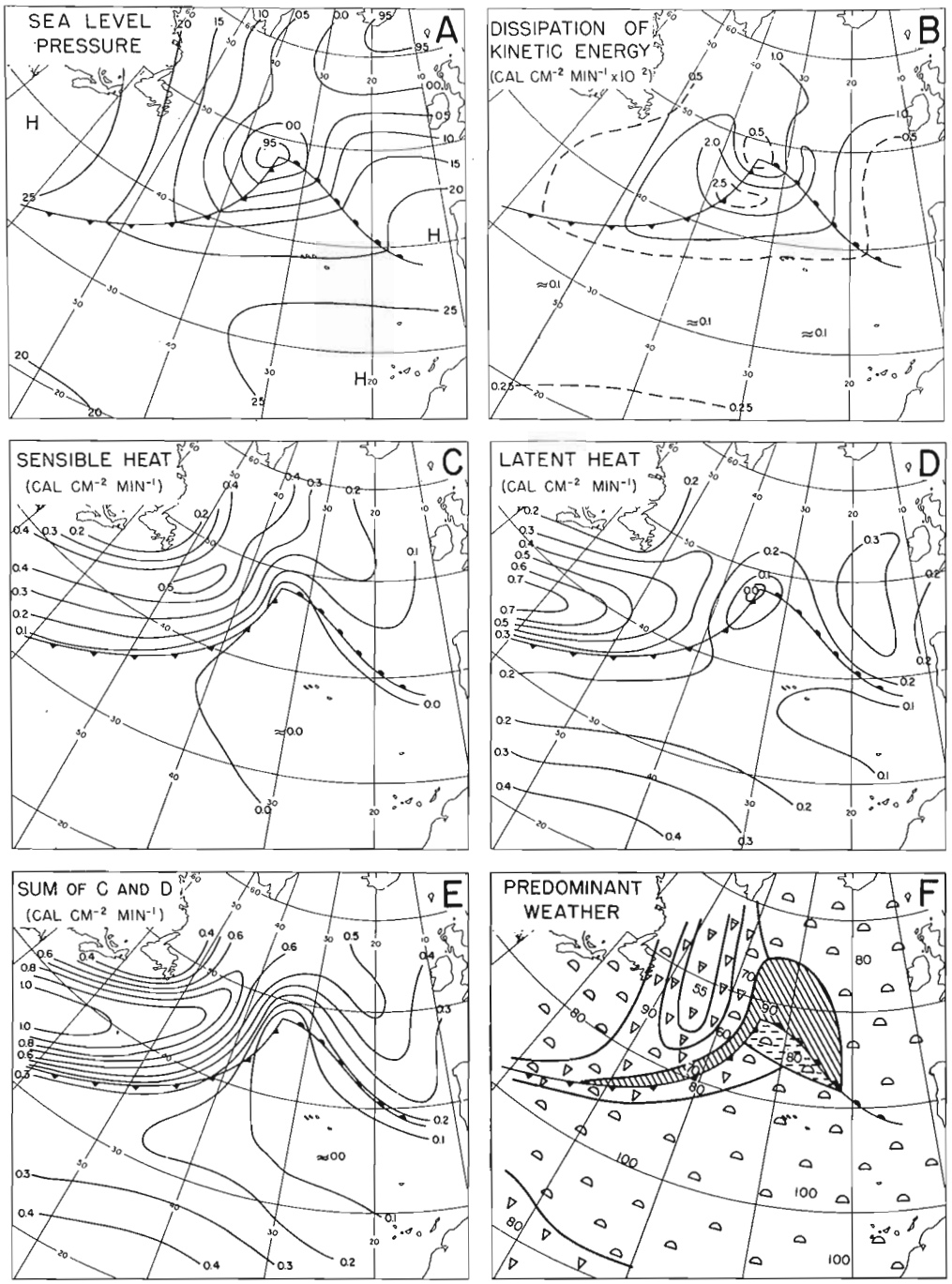

Fig. 4. Models of warm-sector cyclones.

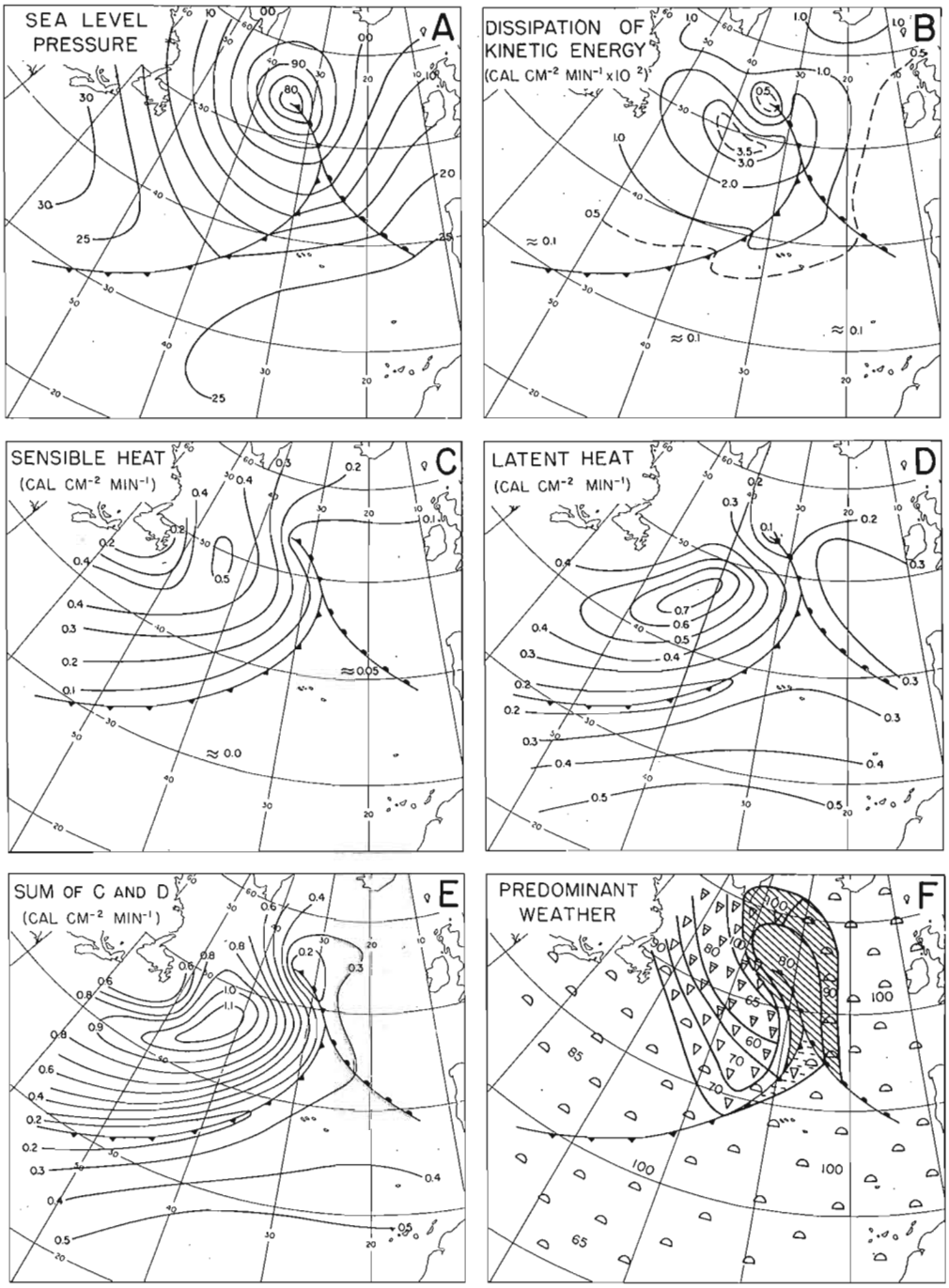

Fig. 5. Models of partly occluded cyclones.

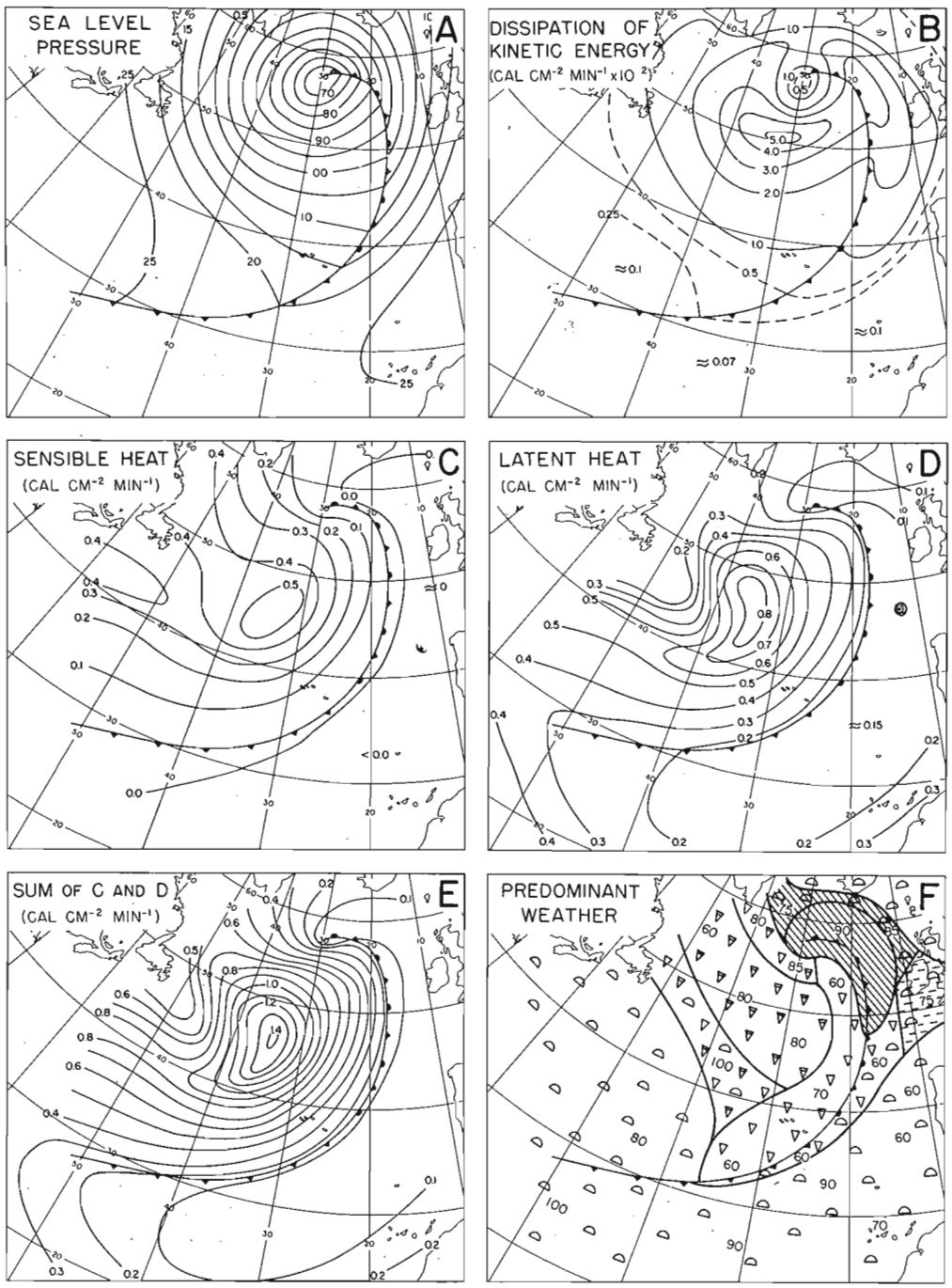

Fig. 6. Models of full occlusions.

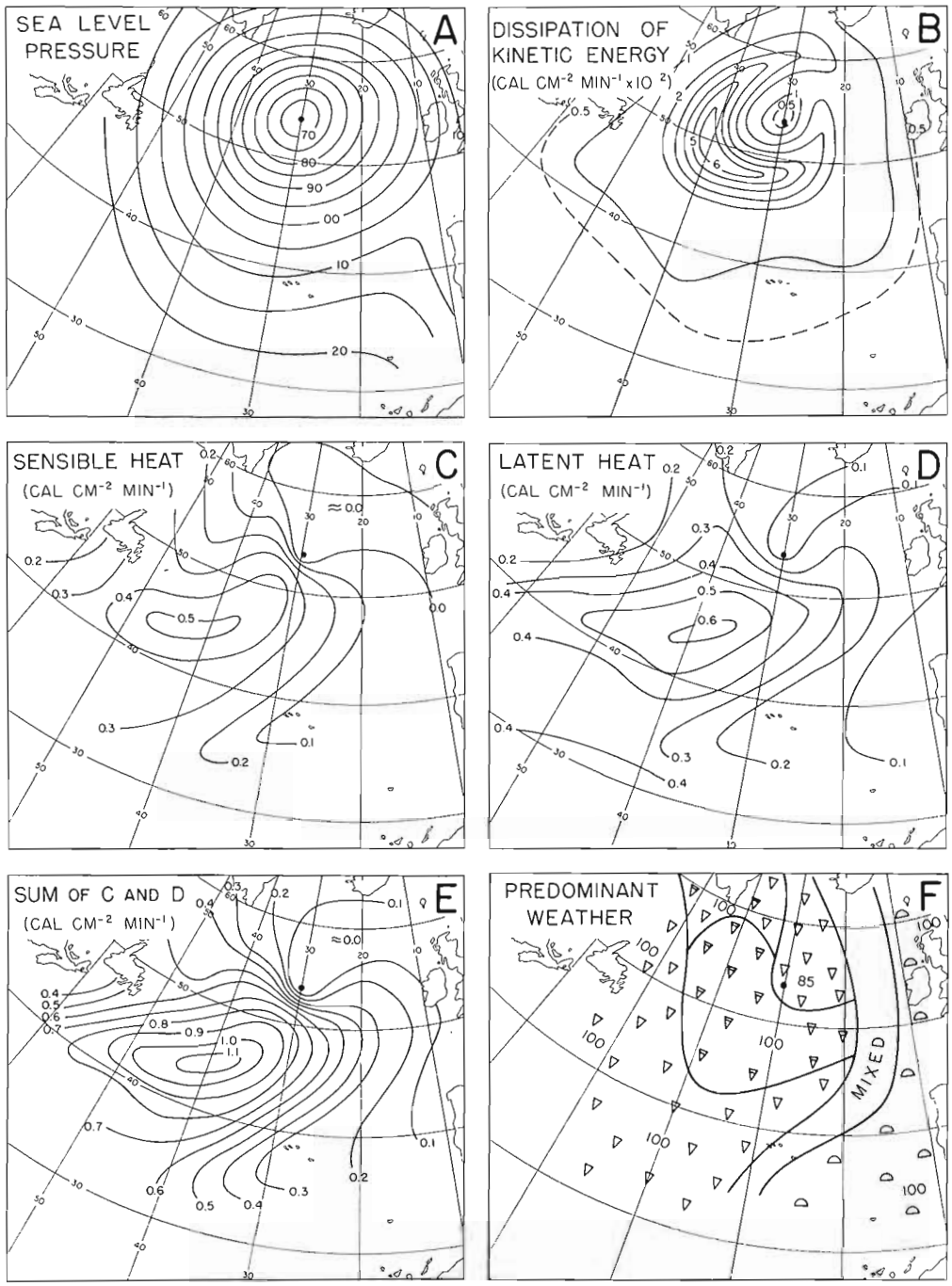

Fig. 7. Models of cold-core frontless cyclones.

to be geostrophic) the isopleths indicate also the general features of the distribution of kinetic energy at low levels. It is noteworthy that, in the case of winter cyclones on the North Atlantic, the largest amount of kinetic energy at low levels is reached at a time when the baroclinic structure has been largely destroyed.

Turning now to the patterns of heat fluxes (Charts C and D) it is of interest to note that the averaging procedure used in the construction of the models tended to reduce the extremes, for in individual cases the maxima were located at somewhat varying distances from the frontal zones and the centers of the disturbances. Typical maxima of the sensible flux (F_S) were about 1 cal cm^{-2} sec^{-1}, and the similar maxima of the flux of latent heat (F_L) were about 1.4 units. Since F_S is proportional to $T_s - T_a$ while F_L is proportional to $e_s - e_a$, large values of F_S are often found over cold coastal waters together with low values of F_L. This is due to the circumstance that the saturation value of e increases rapidly as the temperature increases beyond (say) 5°C, with the results that large values of $e_s - e_a$ will not occur unless the sea-surface temperature is sufficiently high. It will be seen from Charts C and D that, for example, the waters to the east of Labrador contribute very little to the evaporation though their contribution to the sensible heat flux may be very large when the air streams oceanward.

Except over the above-mentioned cold waters, the fluxes F_S and F_L are highly correlated, as can be seen by comparing Charts C and D with Charts E, the last-named group of charts representing the loss of heat by the sea through evaporation and eddy flux of heat into the atmosphere. The upward radiative fluxes, which are generally in the range of 0.00 to 0.10 cal cm^{-2} min^{-1}, will be discussed later. In extreme cases the loss of heat to the atmosphere may exceed 2.5 cal cm^{-2} min^{-1}, which is about 20 times the average absorption of incoming radiation in latitude of 50°N in winter.

It is convenient first to discuss the conditions within the tropical air mass. It will be seen from Charts C in Figs. 3—6 that the air to the south of the developing cyclone wave is very nearly in thermal equilibrium with the ocean surface. Not only is the mean eddy flux of sensible heat close to zero but so are also the individual values.

In Fig. 8 are shown the upward radiative flux of heat at the interface. Though it is difficult to determine the probable errors involved, the configuration of the patterns agree well with what one would expect from considerations of moisture content, cloud cover, sea-surface temperature, etc. It appears, therefore, that the combined effect of eddy and radiative heat fluxes is to supply heat to the warm-sector air. Though the amounts may be small they are nevertheless of interest for the thermal analyses (not reproduced) show clearly that the tropical air that takes part in the circulation of the developing wave cools at a rate of the order of 5°C in 24 hours, while the charts of the heat fluxes (Figs. 3—6, and 8) show that the heat is not surrendered to the ocean.

Some insight into the mechanism of adjustment of the tropical air can be gleaned from the inset diagrams of Fig. 9 and from Charts F of Figs. 3—7. These latter charts show that, except close to the front and deep in the tradewind belt, the state of the sky is characterized by a rather uniform deck of flat cumulus and stratocumulus. This

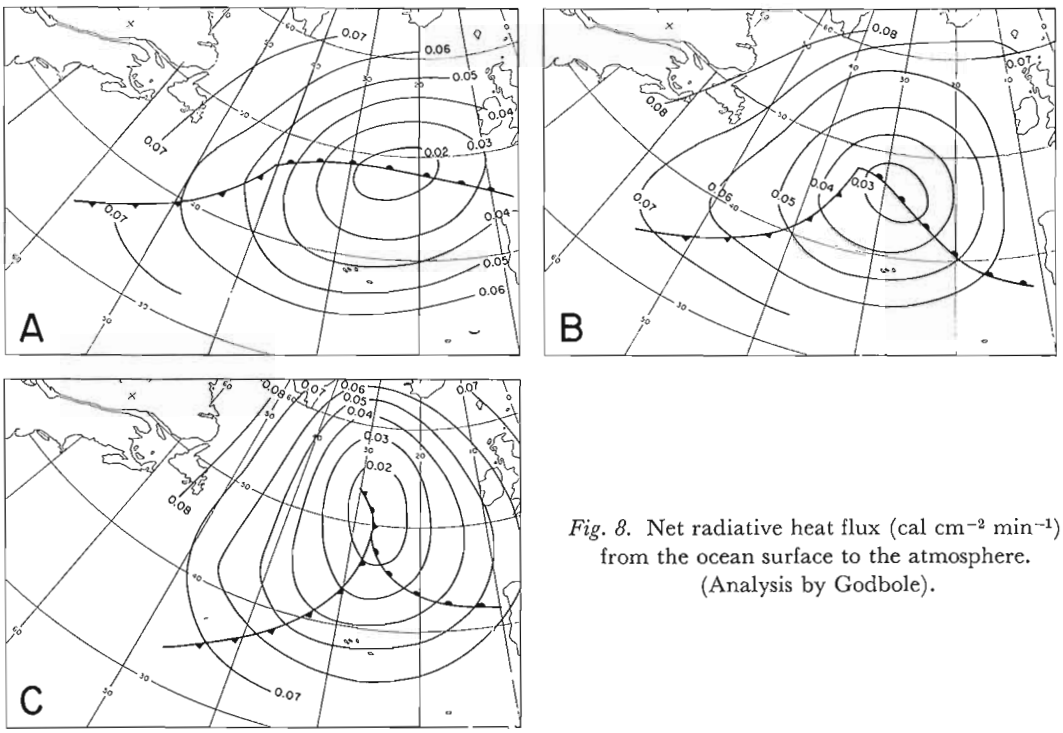

Fig. 8. Net radiative heat flux (cal cm^{-2} min^{-1}) from the ocean surface to the atmosphere. (Analysis by Godbole).

light convective activity is consistent with slight heat flux from the ocean surface, and it is also consistent with the presence of a dry inversion (of which we have general knowledge) above the cloud deck.

It will be seen from Fig. 9 that the distribution along the vertical of the radiative flux is such that a layer with an average rate of cooling of 5 to 6°C a day is present at about 800 mb, and this marks the upper surface of the average cloud deck, or the top of the exchange layer.

The combined effect of the radiative and eddy fluxes at sea level and radiation from the top of the cloudy layer is to remove heat from warm air that takes part in the developing cyclone. The various steps in this adjustment between the sea and the tropical air may be summarized as follows: (a) slight heating from below; (b) eddy transfer of moisture to, and condensation in, the air below the inversion; (c) appreciable loss of heat through radiation from the top of the moist layer; and (d) turbulent redistribution of heat below the inversion so as to satisfy the principle of lapse rate.[1]

It will be seen from Charts D (Figs. 3—6) that the tropical air is steadily supplied with water vapor, and since precipitation is present only along the frontal zone to the north and in the equatorial belt (Charts F, Figs. 3 and 4) the water vapor balance

[1] The net heat flux within the exchange layer will often be against the mean gradient of the potential temperature. See PRIESTLEY and SWINBANK (1947).

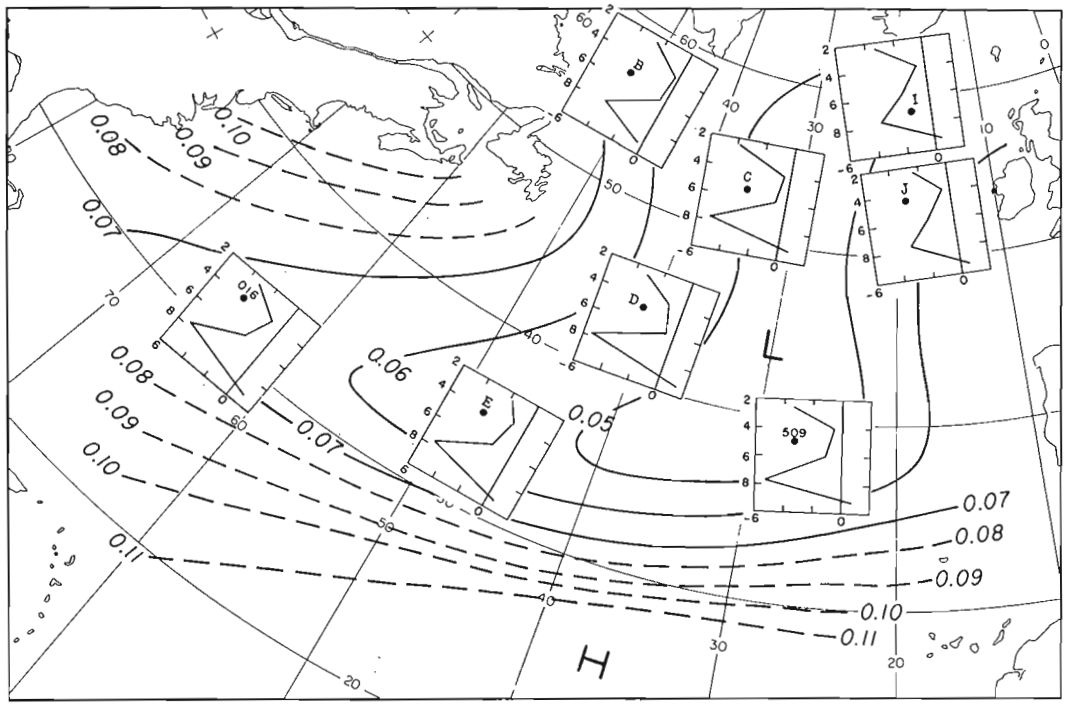

Fig. 9. Net radiative heat flux (cal cm^{-2} min^{-1}) at sea level (broken lines based mainly upon extrapolation). Inset diagrams show the divergence of the heat flux as a function of pressure (8 = 800 mb) and expressed as rate of heating (— 6 = — 6°C) (°C in 24 hours). The chart shows mean values for the winter months 1956—1957. (Analysis by Godbole).

is maintained through horizontal export, that is, the divergence that is necessary to maintain the subtropical anticyclone. Though the data do not permit the establishment of numerical balances, it is evident that much of the frontal precipitation in middle latitudes and almost all of the rainfall in the equatorial zone derive from water evaporated in the subtropical belts.

Turning now to the polar air, to the north of the frontal zone in Fig. 3, it will be seen that vast amounts of sensible heat and latent heat are absorbed by the cold air. Since we are here considering systems with well-developed fronts (through which there can be no appreciable eddy exchange) we must assume that the cold air is the only beneficiary of these heats. Though much of the latent heat is released through condensation in the cold air a considerable portion is accommodated as the cold air absorbs sensible heat. In fact, much of the cold-season precipitation in Europe to the north of the Alps and in Asia to the north of the continental divide, derives from water vapor which the air acquired over the North Atlantic Ocean.

The weather maps (Charts F) are of considerable interest particularly when compared with the heating patterns in Charts C. It is noteworthy that, for example,

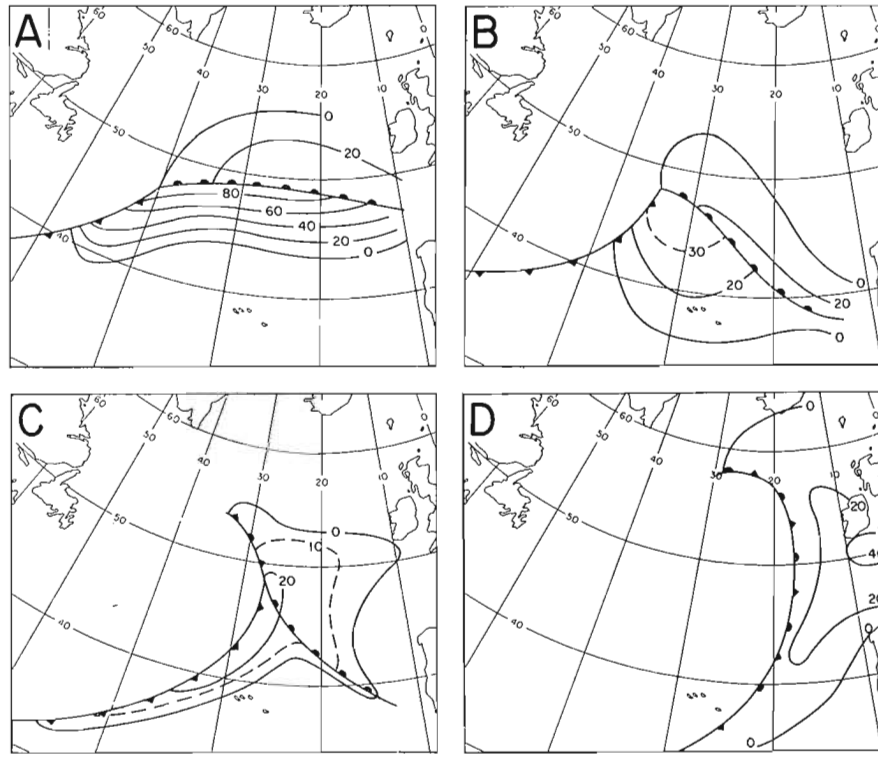

Fig. 10. Percentage probability of occurrence of overcast with fog or low stratus, with or without drizzle.

the axes of the areas with heavy convective activity are oriented more or less at right angles to the axes of the heating patterns. The conditions shown in Fig. 4 are typical. A band of heavy convective activity is present to the northwest of the apex of the wave where the rate of heating is moderate. The convective activity decreases to moderate to the south of Newfoundland where the rate of heating is very large. Still farther to the west only flat cumulus and stratocumulus develop although the supplies of heat and water vapor reach extreme values in this area. The features shown in Fig. 4 are maintained throughout the life history of the model cyclone, except that the area with heavy convective activity increases as the storm moves toward Europe.

By comparing Charts F and A in Figs. 3—7 it will be seen that heating from the underlying surface always results in some convective activity; however, unless the air takes part in a cyclonic circulation, moderate and heavy convection (that is, convection with precipitation) will not occur even if the surface heating is very intense; as far as the state of sky is concerned there is often a larger difference between *cyclonic* and *anticyclonic* air masses than there is between *cold* and *warm* air masses in the meaning used in customary classifications.

Returning again to Chart C in Figs. 3—7 it will be seen that negative (downward)

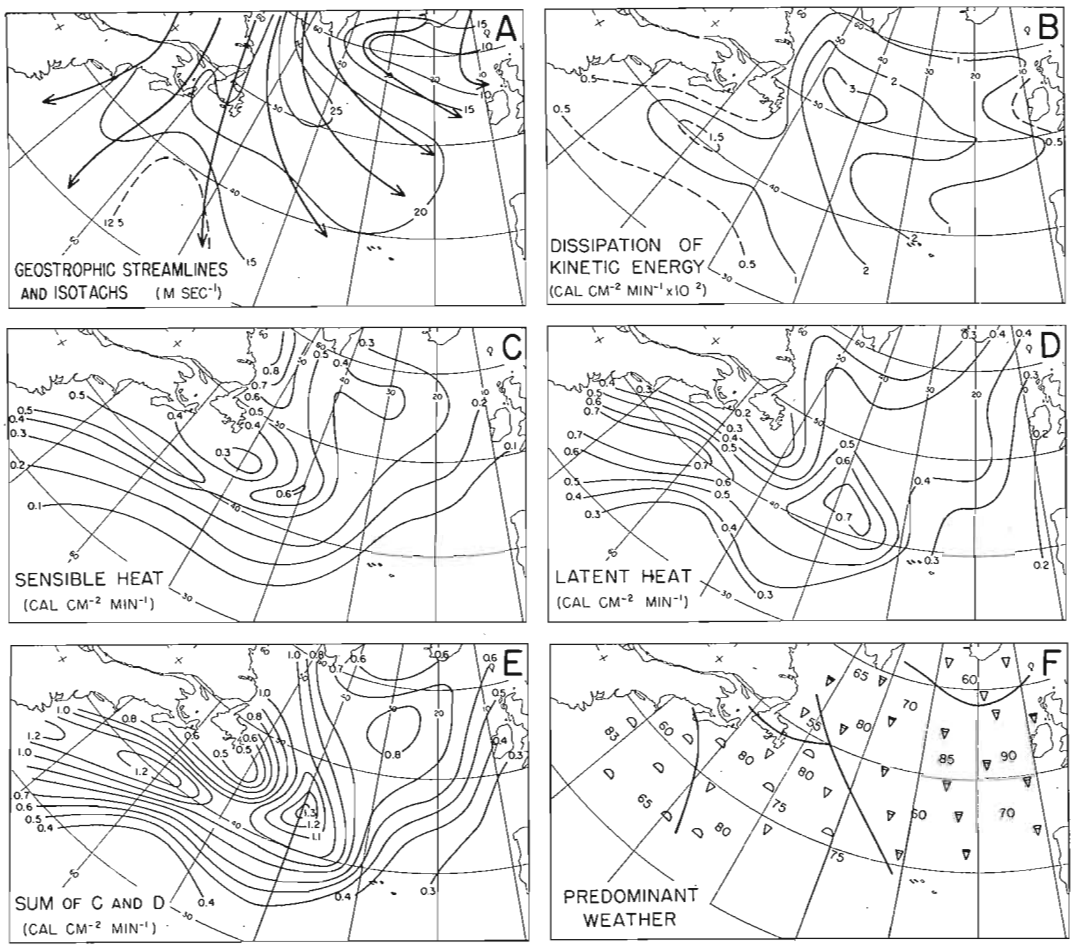

Fig. 11. Composite chart showing the characteristics of outbreaks of arctic air in different parts of the North Atlantic region.

heat fluxes are rare. Within the area enclosed by the zero isopleth the individual values vary slightly about zero with a slight preference for negative values. Individual values less than −0.2 units are exceedingly rare, and when they occur the wind is usually strong. On the whole, overcast sky with low stratus or fog is relatively rare except near the apex of the warm sector and immediately in advance of the warm front. Since overcast with low stratus or fog are rarely sufficiently frequent to qualify as a predominant weather type, the probabilities have been represented separately in Fig. 10. It will be seen that skies of this type are commonly present in the warm air near the apex of the nascent cyclone wave, but as the cyclone develops and the wind increases, the frequency decreases and the area shrinks. In the case of the full occlusion (Chart D) the frequency pattern is probably somewhat influenced by coastal effects.

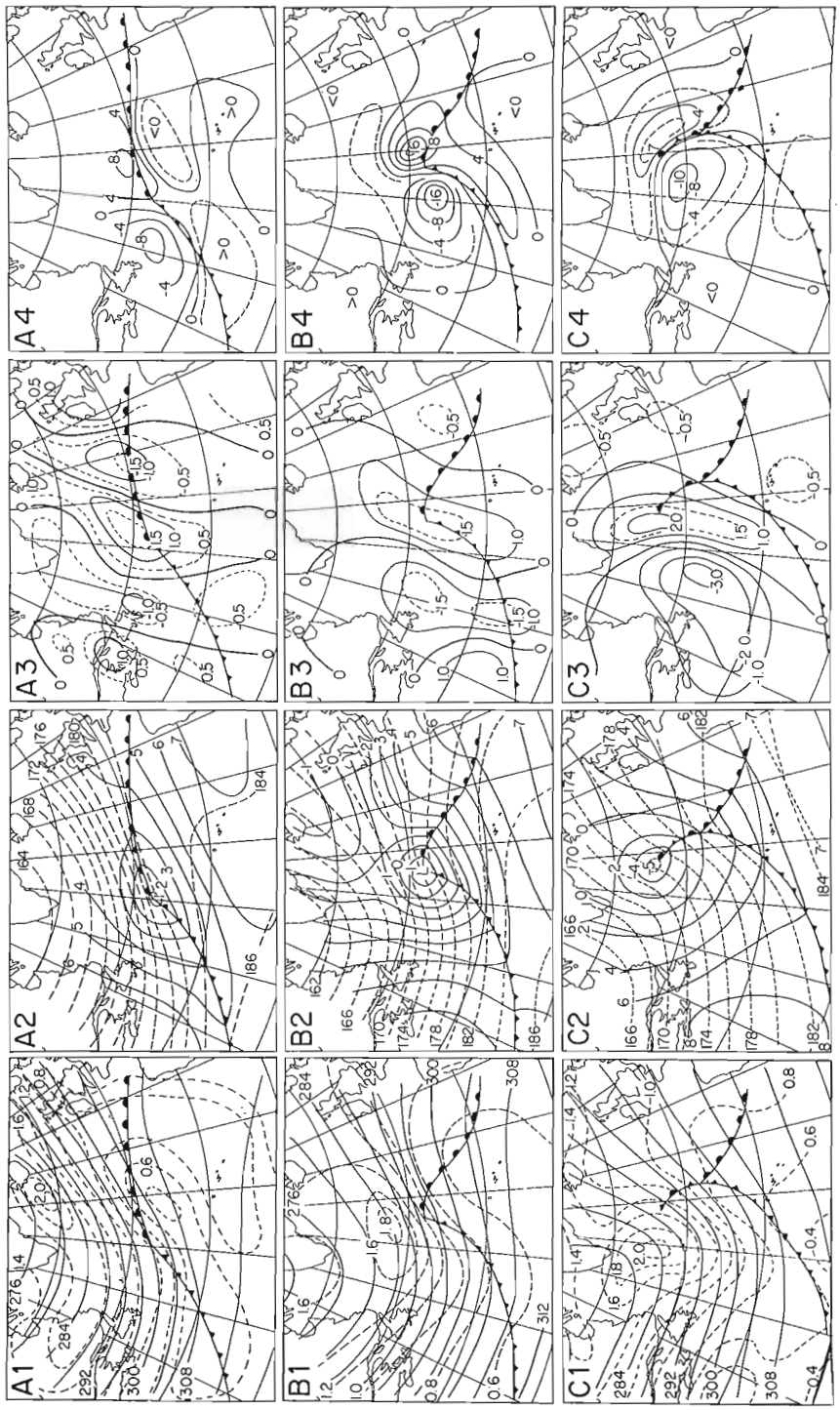

Fig. 12. Continued next page.

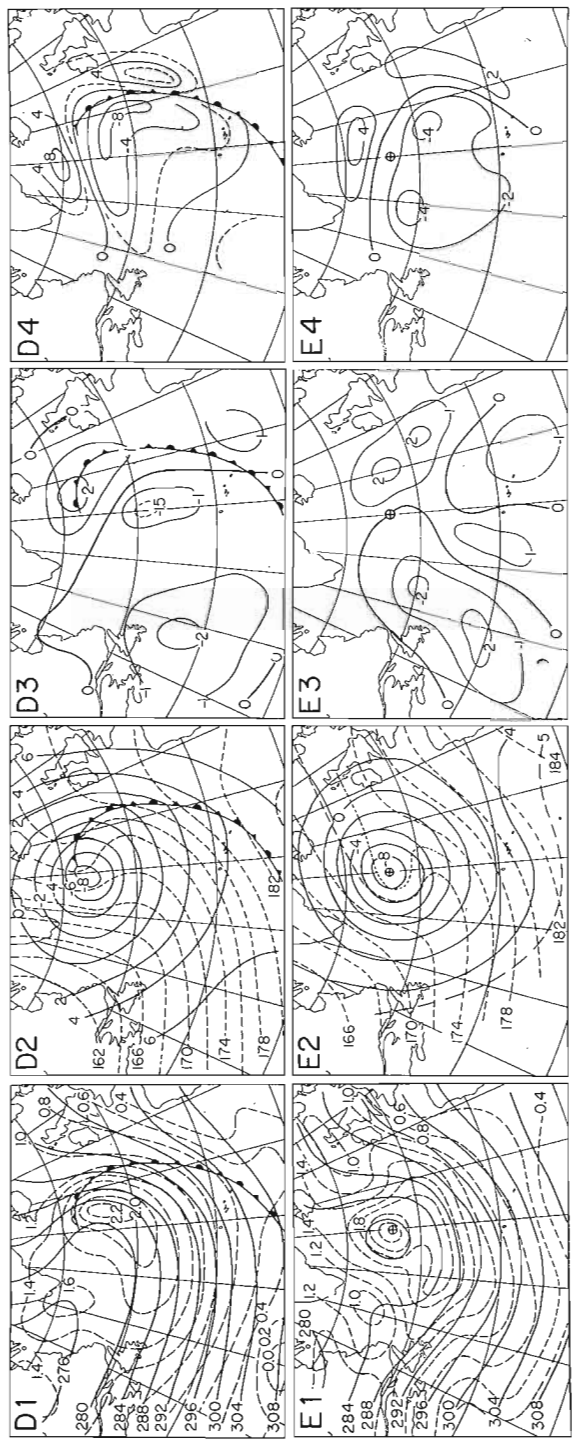

Fig. 12. First column: Fronts at sea level and contours of the 300 mb surface (hundreds of ft) and absolute geostrophic vorticity ($sec^{-1} \times 10^4$). Second column: Contours of 1000 mb surface and thickness from 1000 to 500 mb (hundreds of ft). Third column: Vorticity advection ($sec^{-2} \times 10^8$) at the 300 mb level. Fourth column: The Laplacian of geostrophic thickness advection, multiplied by g/f, in the layer below 500 mb ($sec^{-2} \times 10^8$).

The typical weather conditions associated with outbreaks of arctic air are shown in Fig. 11. In all essentials the conditions resemble those associated with the cold-core low, the main difference being that the area with heavy convective activity is very much larger. A noteworthy feature is the absence of convection with precipitation over the warm waters near the east coast of the United States. Here the outbreaks have an anticyclonic sweep, and deep convection does not develop in spite of the large rate of heating by the Gulf Stream.

2.2. Sequences Aloft. Not much need be said here about the sequences of the vertical structures insofar as absolute and relative isohypses are concerned, for their general features are well known from earlier investigations. Only two aspects invite special comments here, namely, the vorticity advection in the upper troposphere (e.g., at the 300 mb level) and the Laplacian of the thickness advection through the layer below the first level of nondivergence (e.g., below 500 mb). We have chosen these parameters since they have figured prominently in recent discussions of cyclone development (PETTERSSEN, 1955; PETTERSSEN, DUNN, and MEANS, 1955; PETTERSSEN, 1956; HAGE, 1957, 1961). Furthermore, to obtain comparable quantities (see PETTERSSEN, 1955) the Laplacian of the thickness advection has been multiplied by g/f. The results are shown in Fig. 12.

Through a comparison with a large number of similar developments in North America the following differences have become apparent:

A. *North Atlantic Ocean.*

(i) Cyclone development at low levels commences under a more or less straight upper current (without appreciable vorticity advection) in the region where there is a maximum of baroclinicity.

(ii) The upper cold trough develops simultaneously with the low-level cyclone, and the distance of separation between the upper trough and the low-level system remains sensibly unchanged.

(iii) The effect of the vorticity advection aloft is relatively small throughout the development, the major contribution coming from the thermal advection.

B. *North American Continent.*

(i) Cyclone development at low levels occurs normally when a *pre-existing* upper cold trough (with strong vorticity advection on its forward side) approaches a low-level baroclinic zone.

(ii) The distance of separation between the upper trough and the low-level system decreases noticeably during the intensification period, and the axis tends toward a vertical position during the occluded stage.

(iii) At the time of onset of the low-level development, the effect of the vorticity advection aloft is predominant; the effect of the thermal advection increases and becomes overwhelming during the later part of the development.

Cyclone developments of the Atlantic type occur occasionally on the North American Continent. During a forecast experiment conducted in 1955, 8 out of 97 developments in the United States followed the sequence typical of Atlantic cyclones.

From the present data and the results of the several investigations referred to above, it appears plausible that there are two largely different types of cyclone development. The Atlantic type appears to possess some features which are compatible with the SOLBERG-HÖILAND theory of dynamic instability. On the other hand, the customary developments over the North American Continent appear to be initiated by finite disturbances.

3. Numerical estimates. *3.1. Introductory Remarks.* It was shown in the foregoing section that the supply of sensible heat by the ocean surface is normally large, particularly in the rear of mobile cyclones. The same is true also of the supply of latent heat, and though the charts provide no precise information on where this heat is released, much of it must be freed in the cold air in the rear of cyclones where heavy convective activity is prominent. Furthermore, large amounts of latent heat, which were supplied through evaporation in the tradewind belt, are normally released in the warm air above the frontal surface. Finally, one has to consider the loss of heat through radiation from the cloud layers and from the upper troposphere (see Fig. 9). It is evident, therefore, that the effect of heat sources and sinks on cyclone development are essentially complex and need not be small.

In the absence of direct information it has been customary to assume that the effects of heat and cold sources are unimportant except in regard to changes over extended periods of time. Though this is true for the general circulation of the atmosphere, it need not be so for individual systems. The failure of the customary baroclinic prediction models has generally been ascribed to the short-comings of the quasi-geostrophic approximation, truncation errors, etc., rather than to the neglect of sources and sinks of heat. However, there appears to be no foundation in fact for this identification of the sources of errors. On the other hand, the statistical investigation of PETTERSSEN (1950), and the analyses of PETTERSSEN and CALABRESE (1959) clearly indicate that the non-adiabatic effects may be appreciable. The purpose of this chapter is to provide results which may throw some light on the question of the importance of the heat sources and sinks, insofar as cyclone developments are concerned. On account of the very considerable amount of work involved, it has not been possible to perform numerical integrations on such a large number of cases as went into the construction of the models described in Section 2. Instead, it was decided to treat only 10 synoptic situations, with two cases for each of the development stages: the nascent wave, the warm-sector cyclone, the partly occluded cyclone, the fully occluded cyclone, and the frontless cold-core low. Furthermore, and largely as a matter of convenience, it was decided to compute the effect on the change of thickness from the 1000 to the 500 mb surface.

3.2. Basic Equations. It will be assumed that the motion is frictionless and that its time and space scales are sufficiently large for the hydrostatic and quasi-geostrophic approximations to be valid. This latter approximation involves the neglect of the *a*-geostrophic wind without omitting the vertical motion (ω). Furthermore, as is customary in numerical predictions, the relative vorticity (q) is neglected in the term containing the horizontal divergence.

With the symbols defined elsewhere[1] the vorticity equation and the thermodynamic energy equation may be written

$$\frac{g}{f}\frac{\partial}{\partial t}\nabla^2 Z = -\boldsymbol{v}\cdot\nabla\,(q+f) + f\frac{\partial\omega}{\partial p} \tag{3.1}$$

$$g\frac{\partial}{\partial t}\left(\frac{\partial Z}{\partial p}\right) = -g\,\boldsymbol{v}\cdot\nabla\,\frac{\partial Z}{\partial p} - \sigma\omega - \frac{R}{c_p}\frac{H}{p} \tag{3.2}$$

where σ is the stability measure.

Eliminating the time-derivative terms, the following diagnostic equation in ω is obtained.

$$\nabla^2\left[\sigma\omega\right] + f^2\frac{\partial^2\omega}{\partial p^2} = f\frac{\partial}{\partial p}\left[\boldsymbol{v}\cdot\nabla Q\right] - g\nabla^2\left[\boldsymbol{v}\cdot\nabla\,\frac{\partial Z}{\partial p}\right] - \frac{R}{c_p}\nabla^2\frac{H}{p} \tag{3.3}$$

Since this equation is linear in the vertical velocity, we may divide the vertical velocity into components. Thus

$$\omega \equiv \omega_A + \omega_H \tag{3.4}$$

where ω_A is the part that corresponds to dryadiabatic processes, and ω_H is the additional motion due to supply of heat. If desired, ω_H may be subdivided to reflect supply of sensible heat and release of latent heat.

The general diagnostic equation (3.3) now provides two special equations, viz.,

$$\nabla^2\sigma\omega_A + f^2\frac{\partial^2\omega_A}{\partial p^2} = f\frac{\partial}{\partial p}\left[\boldsymbol{v}\cdot\nabla Q\right] - g\nabla^2\left[\boldsymbol{v}\cdot\nabla\,\frac{\partial Z}{\partial p}\right] \tag{3.5}$$

and

$$\nabla^2\sigma\omega_H + f^2\frac{\partial^2\omega_H}{\partial p^2} = -\frac{R}{c_p}\nabla^2\frac{H}{p} \tag{3.6}$$

Substituting (3.4) into (3.2) and integrating between the pressure levels p_5 (= 500 mb) and p_0 (= 1000 mb), we obtain, when Z_T signifies the thickness of the layer

$$g\frac{\partial Z_T}{\partial t} = g\int_5^0 \boldsymbol{v}\cdot\nabla\,\frac{\partial Z}{\partial p}\,\delta p + \int_5^0 \sigma\omega_A\,\delta p + \int_5^0 \sigma\omega_H\,\delta p + \frac{R}{c_p}\int_5^0 \frac{H}{p}\,\delta p \tag{3.7}$$

Here, subscripts 0 and 5 refer to the 1000 and the 500-mb surfaces.

[1] See List of Symbols p. 279.

It is convenient now to divide ω_H into two parts corresponding to the supplies of sensible (S) and release of latent (L) heat. The foregoing equation may then be replaced by the following

$$g\left(\frac{\partial \mathcal{Z}_T}{\partial t}\right)_A = g\int_5^0 \boldsymbol{v}\cdot\nabla\,\frac{\partial \mathcal{Z}}{\partial p}\,\delta p + \int_5^0 \sigma\omega_A\,\delta p \tag{3.8}$$

$$g\left(\frac{\partial \mathcal{Z}_T}{\partial t}\right)_S = \int_5^0 \sigma\omega_S\,\delta p + \frac{R}{c_p}\int_5^0 \frac{H_S}{p}\,\delta p \tag{3.9}$$

$$g\left(\frac{\partial \mathcal{Z}_T}{\partial t}\right)_L = \int_5^0 \sigma\omega_L\,\delta p + \frac{R}{c_p}\int_5^0 \frac{H_L}{p}\,\delta p \tag{3.10}$$

The methods used to evaluate the three components of the thickness tendency are described in the following sections.

3.3. The Thickness Tendency due to Dryadiabatic Motion. The first term on the right of eq. (3.7) may be replaced by

$$-\,g\,\boldsymbol{v}_m\cdot\nabla\mathcal{Z}_T$$

where $\boldsymbol{v}_m$ is some appropriate mean value. In the evaluations to follow we shall approximate the thickness advection by putting $\boldsymbol{v}_m = \boldsymbol{v}_7$, i. e., the wind at the 700 mb level. Thus,

$$g\int_5^0 \boldsymbol{v}\cdot\nabla\,\frac{\partial \mathcal{Z}}{\partial p}\,\delta p = -\,g\,\boldsymbol{v}_7\cdot\nabla\mathcal{Z}_T \tag{3.11}$$

In the construction of certain prediction models, e. g., those of SAWYER and BUSHBY (1953), ESTOQUE (1957), and others, it has been customary to prescribe the ω-profile so as to obtain a monotonic variation from $\omega = 0$ at sea level to a numerical maximum at some specified pressure level. We shall here assume that ω_A has a parabolic profile with zero at 1000 and 200 mb, while ω_S and ω_L are not so restricted. Furthermore, where σ appears together with ω_A it will be replaced by a standard value $\bar{\sigma}$ defined as

$$\bar{\sigma} = \frac{1}{\bar{\omega}_A\,500\,mb}\int_5^0 \sigma\omega_A\,\delta p \tag{3.12}$$

Using the standard-atmosphere value of σ one finds $\bar{\sigma}$ very nearly equal to 2×10^{-4} cgs units.

With the foregoing simplifications eq. (4.8) reduces to

$$\left(\frac{\partial \mathcal{Z}_T}{\partial t}\right)_A = -\,\boldsymbol{v}_7\cdot\nabla\mathcal{Z}_T + \frac{\bar{\sigma}}{g}\,\bar{\omega}_A \tag{3.13}$$

3.4. The Thickness Tendency due to Sensible Heat. The analyses presented in Section 3 provide some information on the flux (F_S) of sensible heat through the base of an air column of unit cross section. In order to calculate the effect of this flux on the thickness Z_T, knowledge of the distribution of F_S as a function of p is required. It will be assumed that there is an upper level p_u at which the flux F_S is a small fraction of the flux F_0 at sea level, so that the depth of penetration is $p_0 - p_u$, with $p_0 \approx 1000$ mb. Furthermore, it will be assumed that the flux decreases linearly with pressure, such that

$$F_S = F_0 \frac{p - p_u}{p_0 - p_u} \tag{3.14}$$

The heat supplied to a unit mass is expressed by

$$H = g \frac{\partial F}{\partial p} = g \frac{F_0}{p_0 - p_u} \tag{3.15}$$

which may be substituted into eq. (3.9).

The first term on the right of (3.9) may be eliminated on the following arguments. According to the findings in Section 2, appreciable values of F_S are found only in the cold air in the rear of cyclones where the winds are moderate to strong. In these regions σ is very nearly zero from sea level to the cloud base, and since the temperature in the rear of winter cyclones is low, σ is relatively small above the cloud base. For convenience in the evaluation the depth of penetration has been chosen such that $p_u = 700$ mb, and σ has been assumed to be zero below this level. With this simplification the first integral on the right of eq. (3.9) vanishes, and the equation reduces to

$$\left(\frac{\partial Z_T}{\partial t}\right)_S = \frac{R}{g c_p} \int_S^0 \frac{H_S}{p} \delta p = \frac{R}{c_p} \cdot \frac{F_0}{p_0 - p_u} \log \frac{p_0}{p_u} \tag{3.16}$$

where F_0 is computed as shown in the Appendix.

It may be noted that the assumption that $\sigma = 0$ below p_u is consistent with the linear form of F, for it can be shown that if heat is absorbed in a layer of neutral equilibrium the heat flux must be quasi-linear if neutral stability is to be maintained.

Referring back to the discussion in Section 3.3 it should be mentioned that the use of a standard value of σ there does not invalidate the foregoing statement, for ω_A has its maximum above 700 mb while ω_S has its maximum below this level.

Formula (3.16) may be taken to state that to $F_0 = 1$ cal cm^{-2} min^{-1} corresponds a thickness change of 82 ft. in 3 hours, and this is the standard value used in the following. It is of interest to note that if p_u is varied the second term on the right of (3.9) gives the following values for the thickness change in 3 hours

p_u	900	700	500
$\partial Z_T/\partial t$	71	82	115

The standard value, therefore, appears to be satisfactory.

3.5. The Thickness Tendency due to Released Latent Heat. The latent heat released by condensation (H_L) is expressed by

$$H_L = -L\frac{dr}{dt} = -L\frac{dr}{dp}\left(\frac{dp}{dt}\right)_s \tag{3.17}$$

Here, $(dp/dt)_s$ is the individual rate of change of pressure of the air in the saturated (s) state. The other notations have been defined in List of Symbols.

It is now useful to introduce a vertical velocity (ω_E) defined such that

$$\left(\frac{dp}{dt}\right)_s = \omega_E + \omega_L \tag{3.18}$$

where ω_E may be called the effective vertical velocity. If the whole ascent (over the time interval $\triangle t$) is saturated, $\omega_E = \omega_A$. However, if part of the ascent is dry, ω_E is a measure of the appropriate fraction of ω_A. With this substitution, equation (3.17) is written:

$$H_L = -L\frac{dr}{dp}(\omega_E + \omega_L) \tag{3.19}$$

which combined with (3.6) gives

$$\nabla^2(\sigma - \sigma_s)\,\omega_L + f^2\frac{\partial^2\omega_L}{\partial p^2} = \nabla^2\,\sigma_s\omega_E \tag{3.20}$$

where

$$\sigma_s \equiv \frac{R}{c_p}\frac{L}{p}\frac{dr}{dp} \tag{3.21}$$

It will be seen that the introduction of the effective vertical velocity makes it unnecessary to resort to a reiteration procedure to determine ω_L, as was done by Smebye (1958) and others, for ω_E is obtained from the observed moisture distribution after ω_A has been determined.

It may be noted that $\sigma - \sigma_s$ is a measure of the stability in respect of saturated-adiabatic lapse rate. Also, if equation (3.20) is to be used generally, one has to put $\sigma_s = 0$ in the unsaturated regions.

Equation (3.20) may be solved in a manner developed by Pedersen (1961) and the results inserted into (3.10) to give the thickness tendency due to released latent heat. However, in view of the approximations used in Section 3.3, these refinements would add little to the accuracy of our numerical estimates. The procedure used here is as follows. As in Section 3.3, the lapse rate was assumed to be that of the U. S. Standard atmosphere. The stability factor $\sigma - \sigma_s$ was found to be so small in comparison to σ that the difference could be ignored. With this simplification equation (3.10) reduces to

$$g\left(\frac{\partial Z_T}{\partial t}\right)_L = \int_5^0(\sigma - \sigma_s)\,\omega_L\,\delta p - \int_5^0\sigma_s\omega_E\,\delta p = -\int_5^0\overline{\sigma}\omega_E\,\delta p \tag{3.22}$$

where $\overline{\sigma}$ is defined in Section 3.3.

In the evaluations the conditions at the 700 mb level were used to determine where condensation would occur. This level was used also by SMEBYE (1958), and the analyses described in Section 2 seem to indicate that this is the lowest standard isobaric level at which the moisture distribution is representative of the large-scale vertical motions.

Finally, it should be mentioned that there must be compensating (downward) currents corresponding to upward values of ω_L in the saturated regions. The integration procedure provided by PEDERSEN (1961) permits the determination of these descending currents. However, in the present evaluations it was assumed that the regions of descent were so much larger than the regions of ascent that the downward values of ω_L could be ignored. Again, the humidity analyses of the cyclone models described in Section 2 (not reproduced) seemed to suggest that this assumption is broadly valid.

3.6. Diagnostic Computations. The results of these computations are shown in two series of charts (Figs. 13—17 and 18—22) which have been chosen so as to provide typical stages of cyclone development and as much historical continuity as possible within each series. On the whole the cases chosen contained rather small amounts of precipitation due to large-scale vertical motion, with the result that the corrections due to released latent heat are rather smaller than normal. An exception is shown in Fig. 21 where the wave disturbance near Cape Hatteras produced appreciable amounts.

It should be noted that the procedure described in Section 3.5 does not account for the latent heat released as a result of cumulus convection. In many of the cases treated the convective activity was intense; as a result one finds that, on the whole, the errors in the computed tendencies are largest in the rear of the cyclones.

A case of considerable interest is contained in Figs. 13 and 14 which show the development of a slowly amplifying wave. In both stages the addition of the effects of heat sources improved very considerably the prediction based upon the adiabatic assumption. In Fig. 14 the convective activity is heavy between Nova Scotia and Bermuda, and some allowance for additional release of latent heat would have reduced the error in that area.

Another interesting case, with historical continuity, is shown in Figs. 15—17. Though the heat sources here are quite weak the inclusion of their effects clearly improved the prediction.

The second series is shown in Figs. 18—22. A noteworthy feature is a nascent wave (Fig. 18) which moves northeastward and amplifies (Fig. 19) at a moderate rate. It will be seen from Fig. 18 that the adiabatic assumption grossly overestimates the decrease in thickness between 60 and 70° West. The addition of heat sources lead to a considerable improvement upon the adiabatic prediction. The same is true also of Fig. 19.

Fig. 20 shows very large discrepancies between observed and computed adiabatic thickness changes. For example, near Cape Hatteras the adiabatic change is — 200 ft.

while the change due to the heat source is + 160 ft. The addition of non-adiabatic effects led to considerable improvement.

The case which reported large amounts of observed precipitation was that shown in Fig. 21. Here the effect of released latent heat was quite large and resulted in considerable improvement.

In the cold low shown in Fig. 22 the heating patterns are generally weak and disorganized. Nevertheless, their contribution tended to reduce the error of the adiabatic prediction.

In summary, it may be said that the inclusion of the effects of sensible heat fluxes and release of latent heat led to improvement in each of the ten cases.

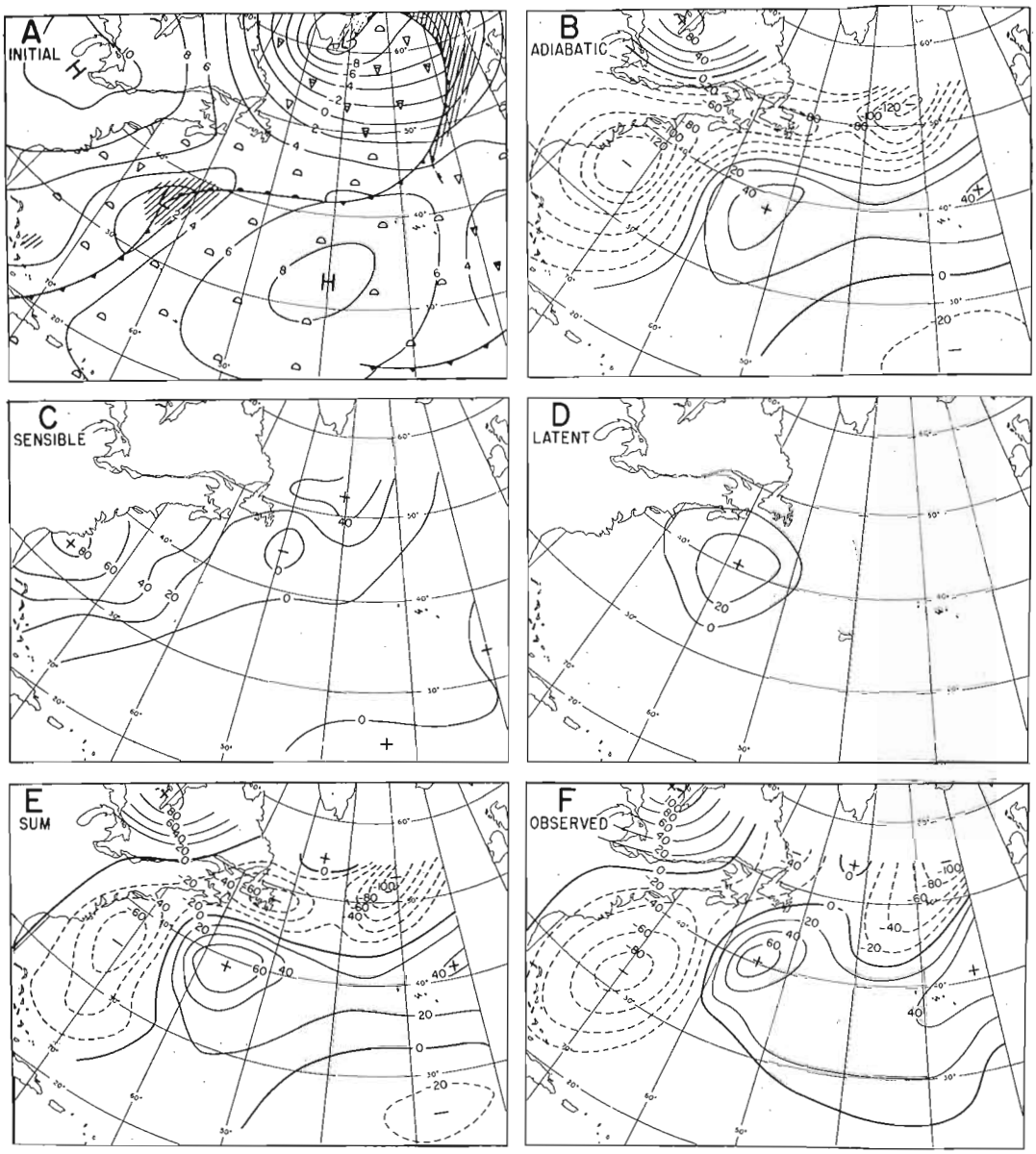

Fig. 13. Computation of 3-hr change of the thickness from 1000 to 500 mb. Nascent cyclone wave, January 4, 1958, 1200 GCT. The charts show: A — weather regions, fronts, and the contours of the 1000 mb surface (hundreds of ft); B — the thickness change (ft) due to adiabatic motion; C — the thickness change due to the flux of sensible heat from the ocean surface; D — the thickness change due to release of latent heat; E — the sum of B, C, and D; F — the observed thickness change.

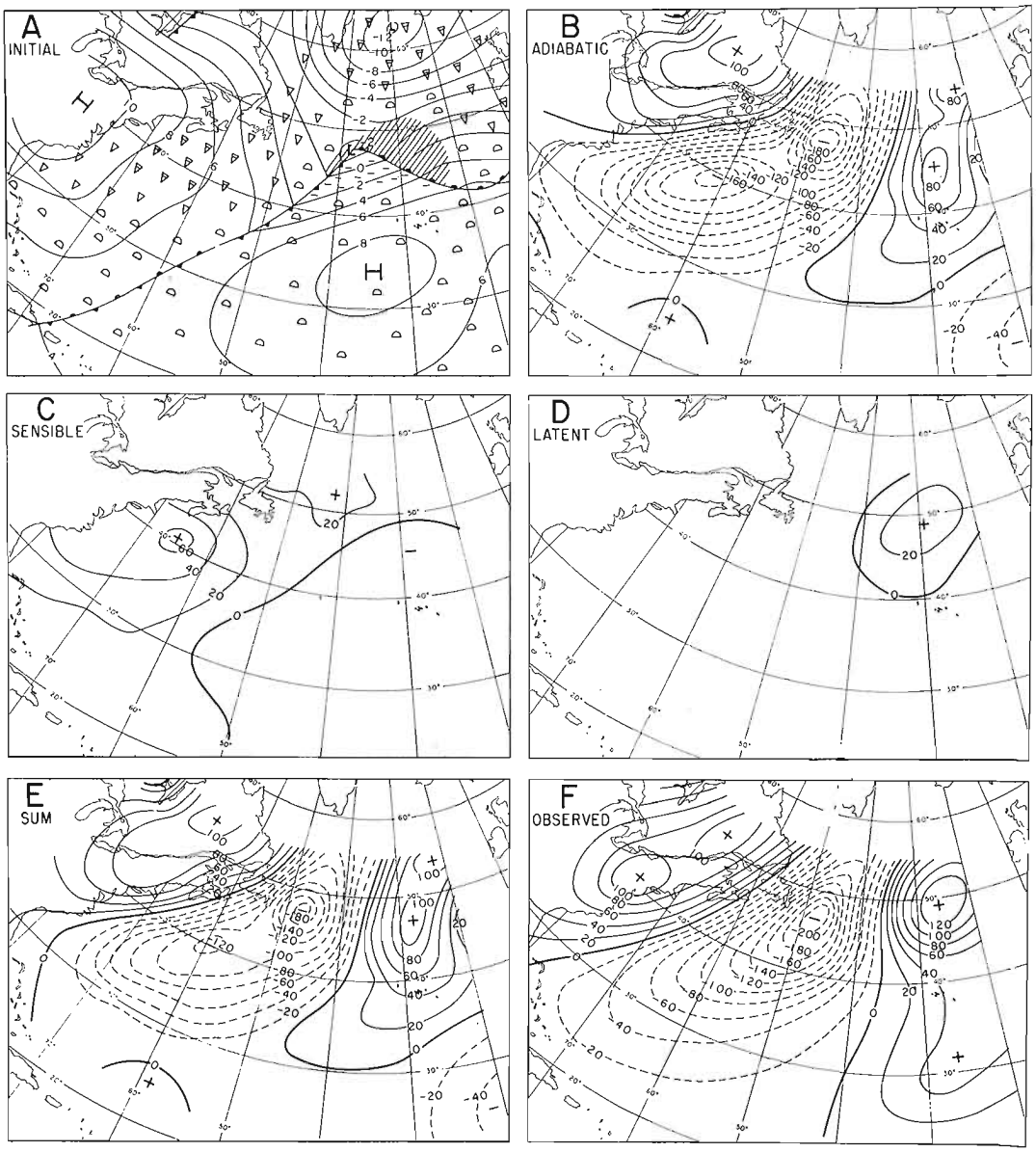

Fig. 14. Computation of 3-hr change in the thickness from 1000 to 500 mb. Warm-sector cyclone, January 5, 1958, 1200 GCT (continued from Fig. 13). Symbols as in Fig. 13.

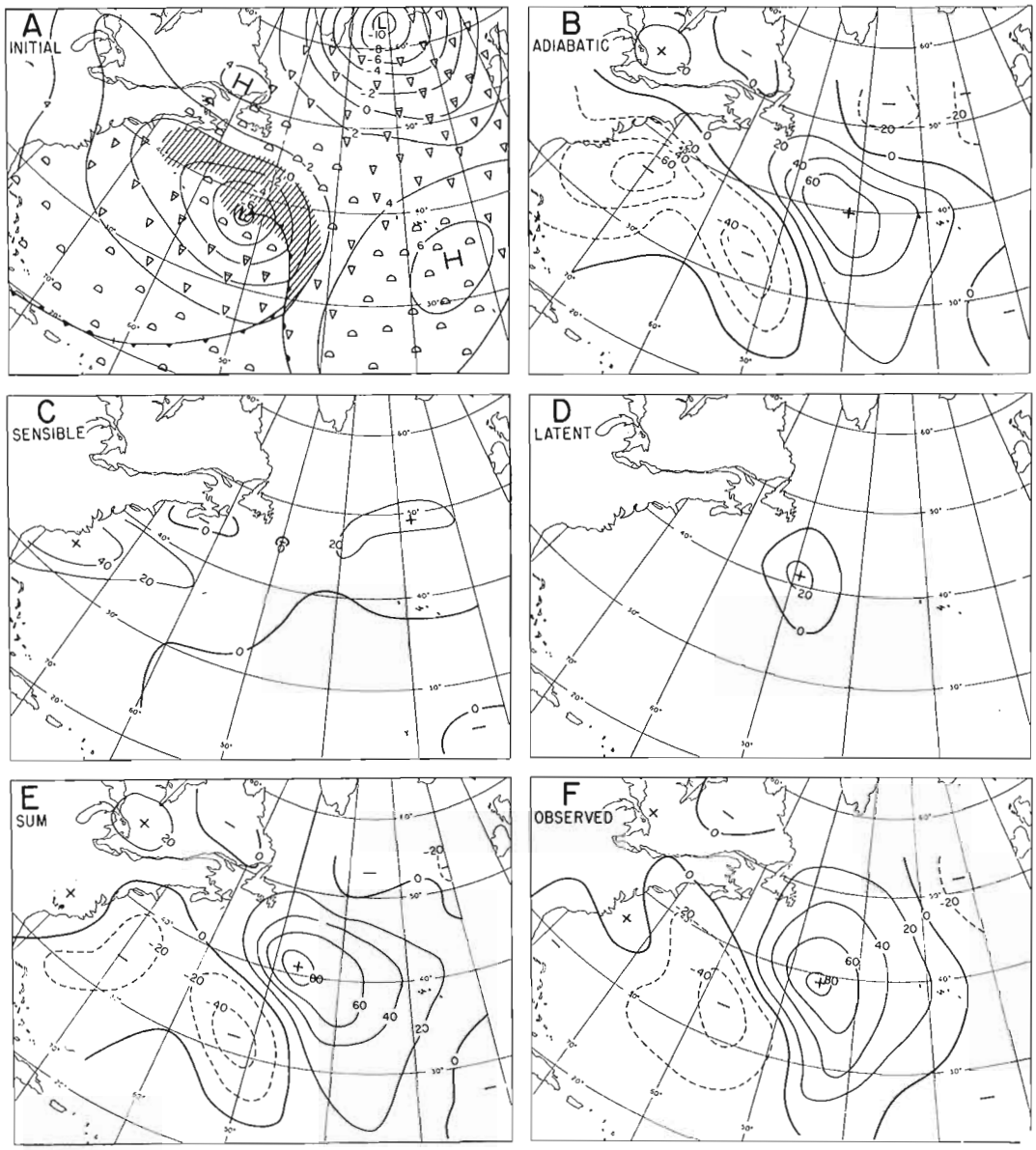

Fig. 15. Computation of 3-hr change in the thickness from 1000 to 500 mb. Partly occluded cyclone, January 28, 1958, 1200 GCT. Symbols as in Fig. 13.

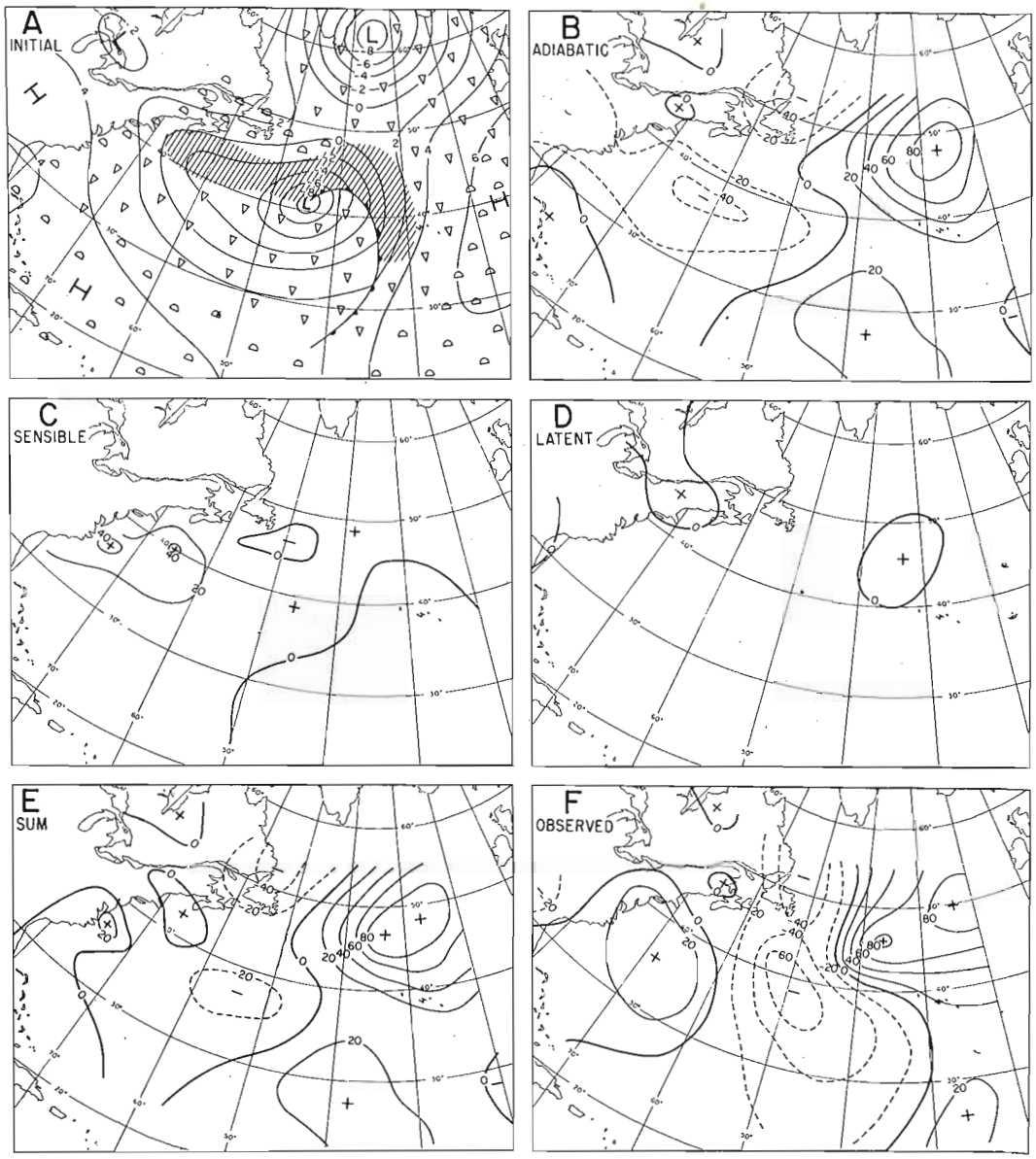

Fig. 16. Computation of 3-hr change in thickness from 1000 to 500 mb. Fully occluded cyclone, January 29, 1958, 1200 GCT (continued from Fig. 15). Symbols as in Fig. 13.

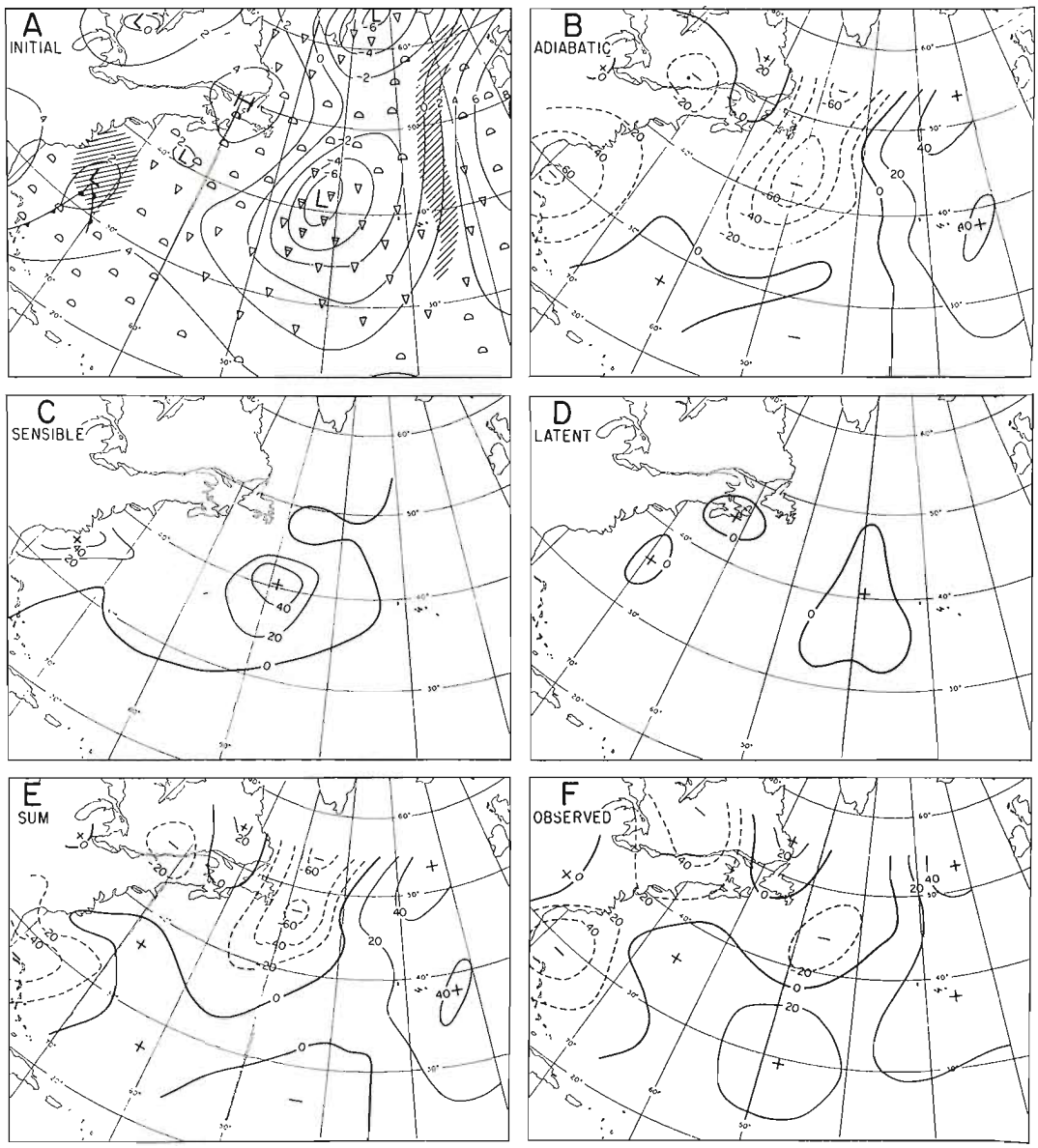

Fig. 17. Computation of 3-hr change in the thickness from 1000 to 500 mb. Cold-core frontless cyclone, January 30, 1958, 1200 GCT (continued from Fig. 16). Symbols as in Fig. 13.

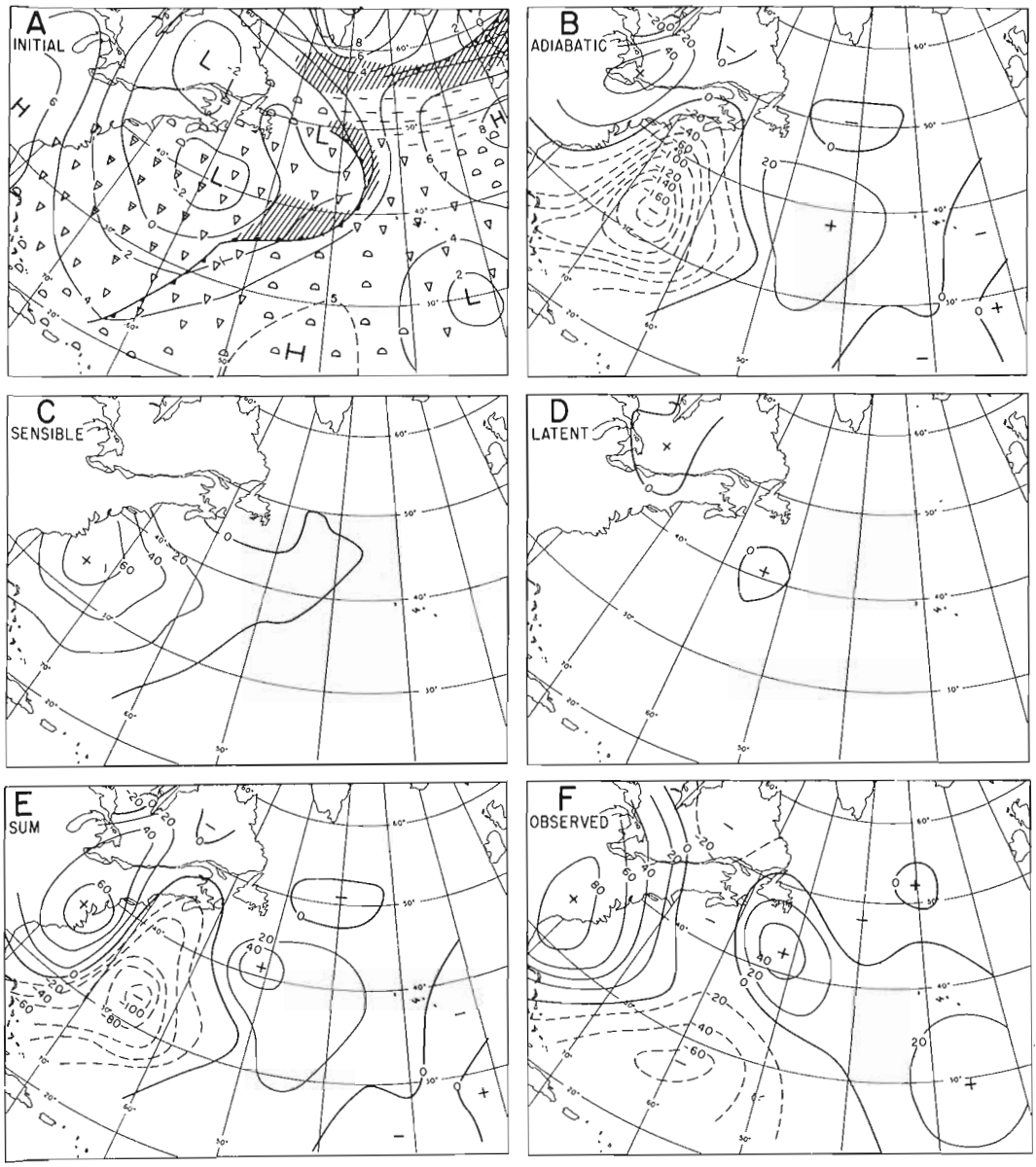

Fig. 18. Computation of 3-hr change in the thickness from 1000 to 500 mb. Nascent cyclone wave, February 4, 1958, 1200 GCT. Symbols as in Fig. 13.

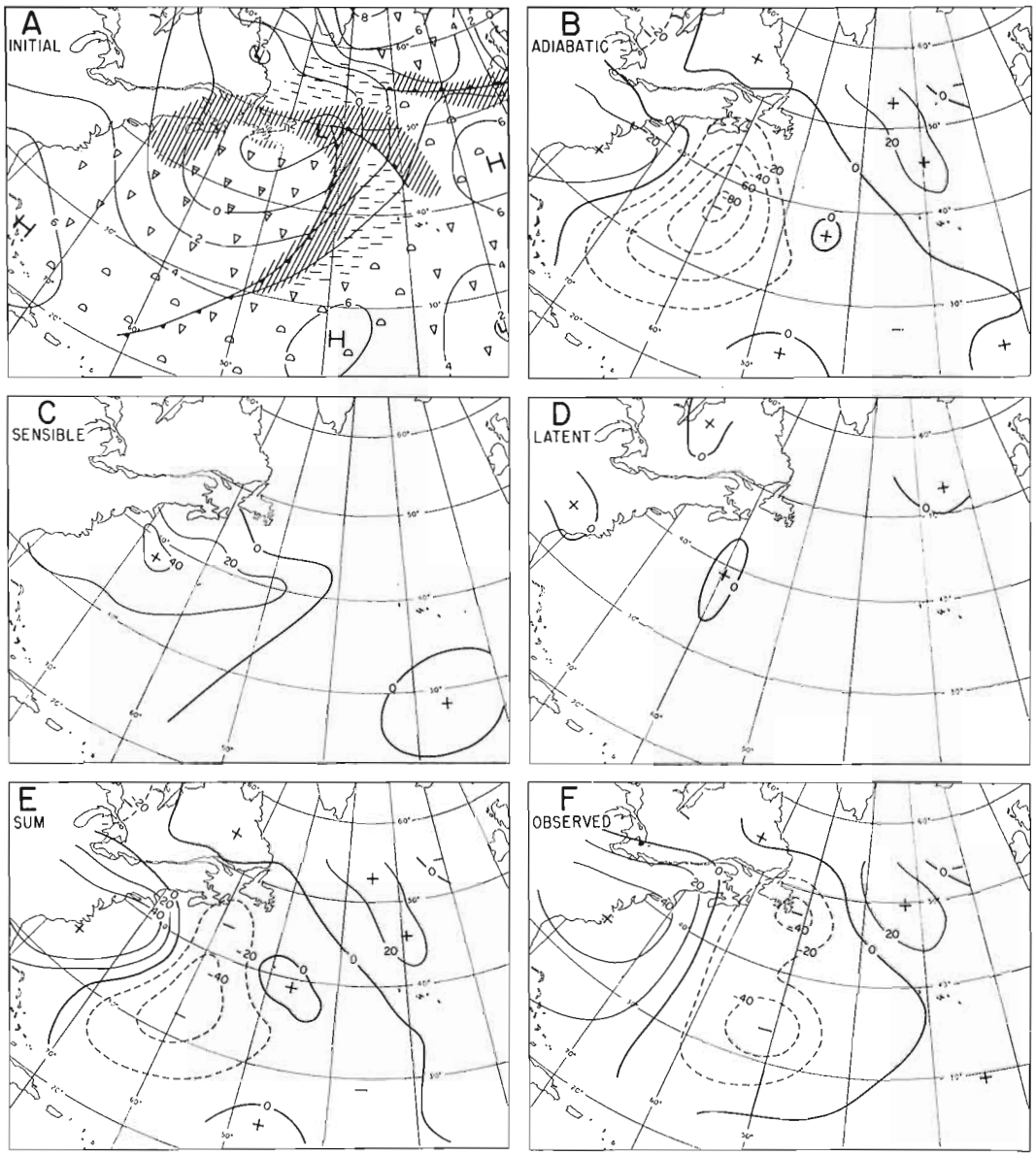

Fig. 19. Computation of 3-hr change in the thickness from 1000 to 500 mb. Warm-sector cyclone, February 5, 1958, 1200 GCT (continued from Fig. 18). Symbols as in Fig. 13.

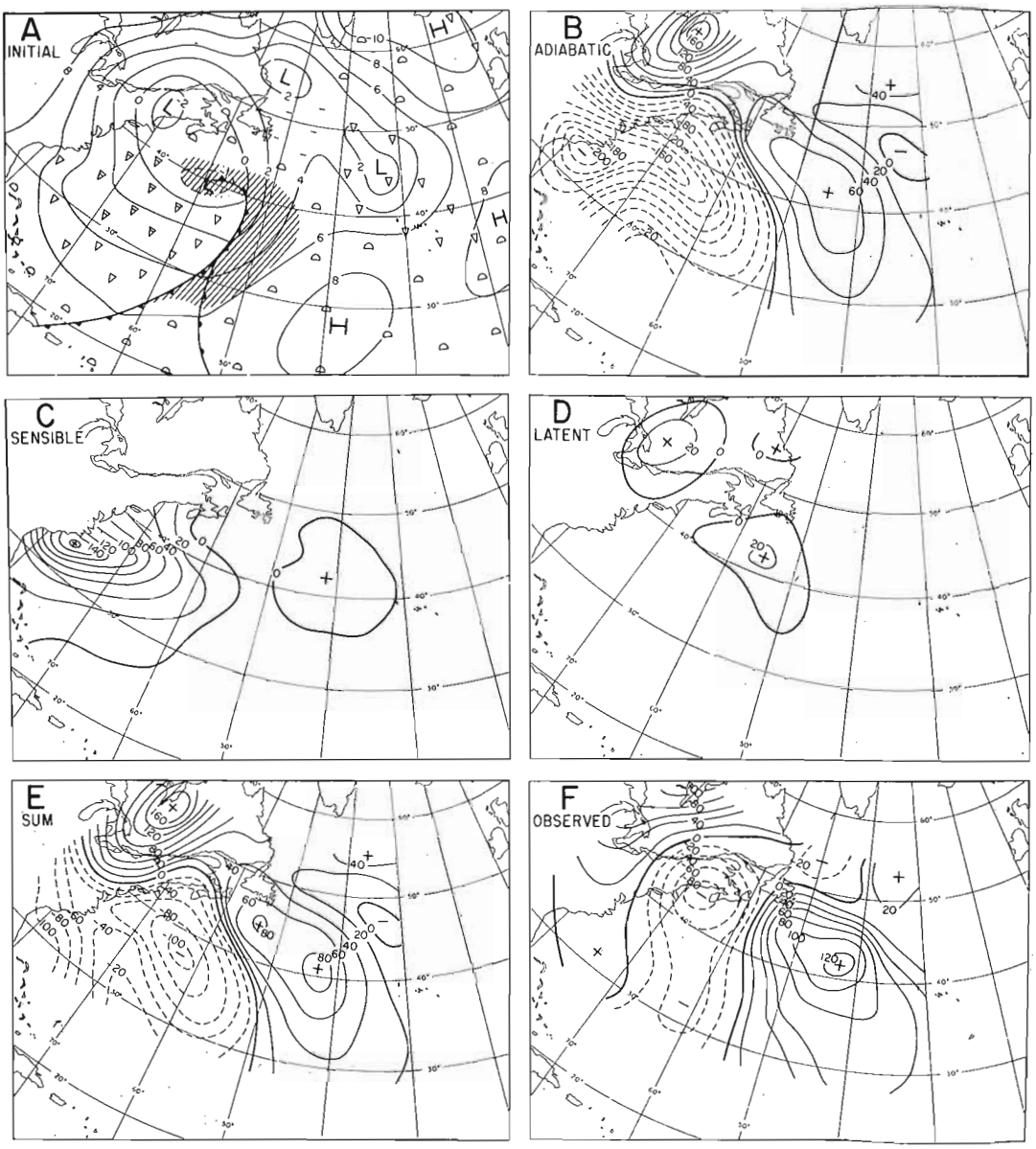

Fig. 20. Computation of 3-hr change in the thickness from 1000 to 500 mb. Partly occluded cyclone, February 17, 1958, 1200 GCT. Symbols as in Fig. 13.

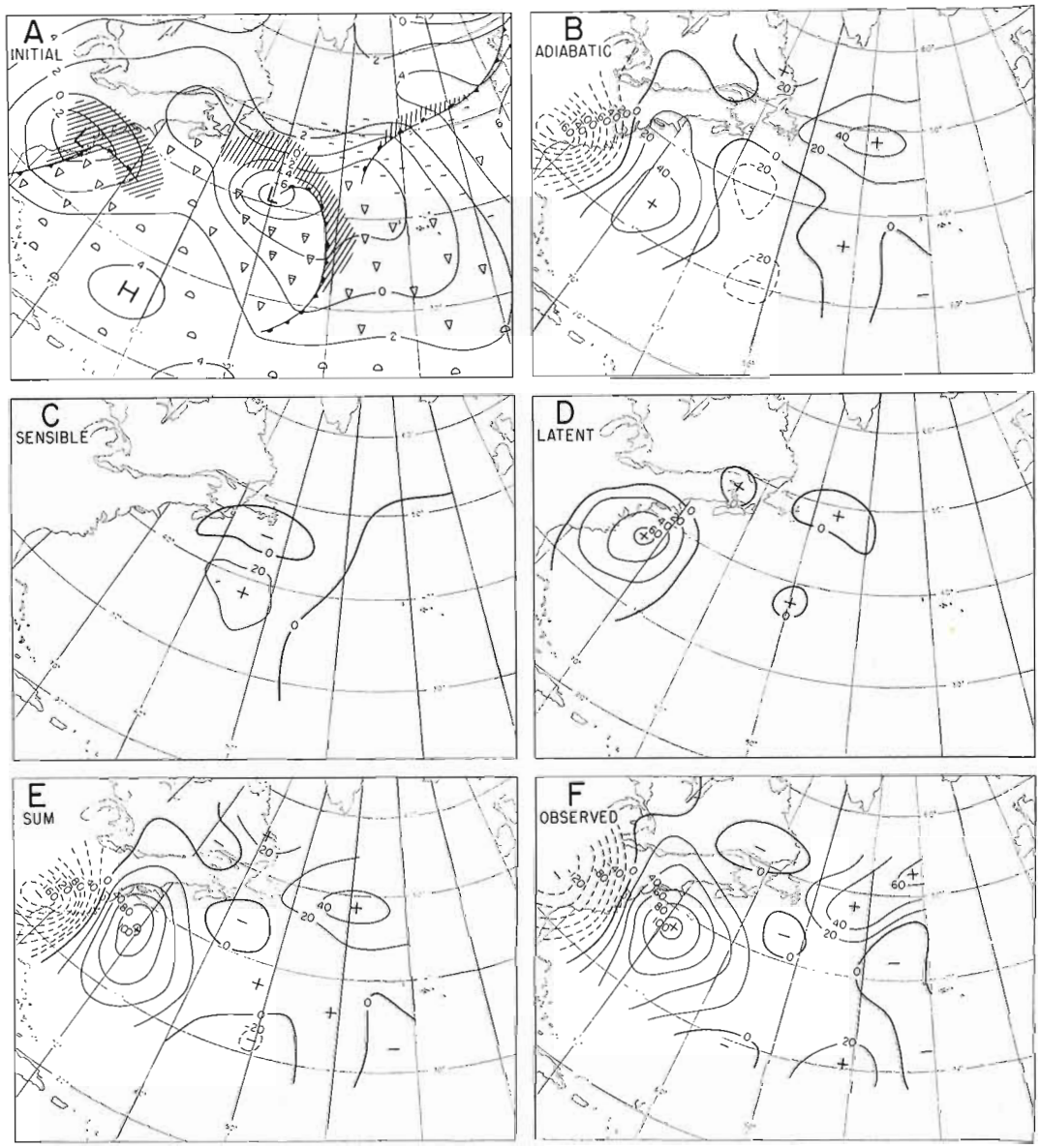

Fig. 21. Computation of 3-hr change in the thickness from 1000 to 500 mb. Fully occluded cyclone, February 1, 1958, 1200 GCT. Symbols as in Fig. 13.

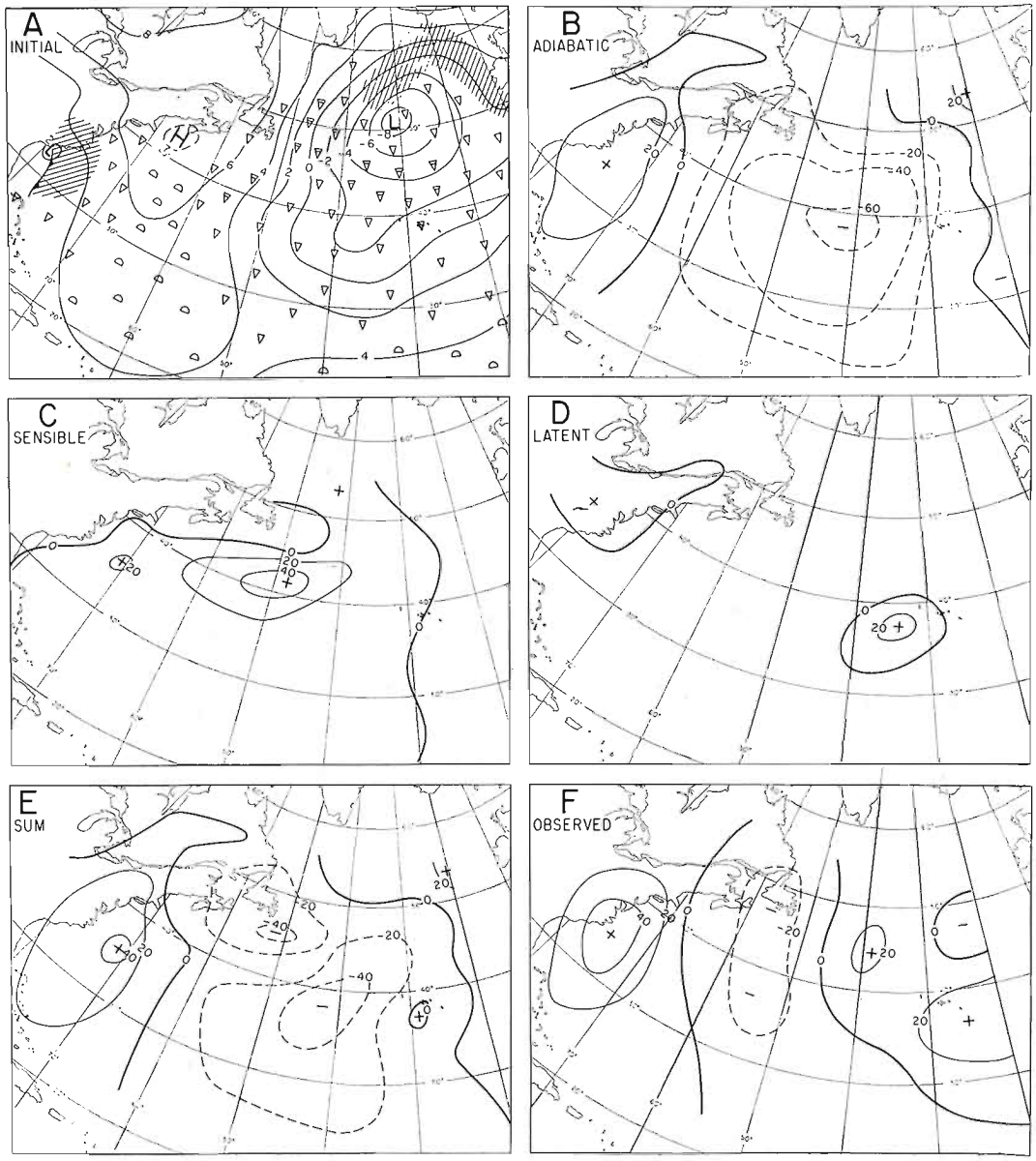

Fig. 22. Computation of 3-hr change in the thickness from 1000 to 500 mb. Cold-core frontless cyclone, March 25, 1958, 1200 GCT. Symbols as in Fig. 13.

APPENDIX

FORMULAE AND EVALUATIONS

1. Eddy Fluxes. From a theoretical point of view the most satisfactory formula for transfer of sensible heat at the ocean-atmosphere interface is, perhaps, the one proposed by SHEPPARD (1958). With the symbols defined in Appendix 2, the formula may be written.

$$F_S = \frac{\varrho c_p k C^{1/2}}{\log\,(k u_* a/\varkappa)}\, V_a\,(T_s - T_a) \tag{1}$$

where subscript s refers to the conditions at the surface, and a signifies the height at which the wind, temperature, etc. are measured.

From investigations by JACOBS (1942) it appears that the quantity

$$\varrho c_p k C^{1/2}/\log\,(k u_* a/\varkappa)$$

may be regarded as a constant, such that

$$F_S = 4.7 \times 10^{-3}\, V_a\,(T_s - T_a) \text{ cal cm}^{-2} \text{ min}^{-1} \tag{2}$$

where V is expressed in m sec^{-1}, and T in °C.

This formula, which has stood up to tests by BURKE (1945) and others, was used in the present investigation. Some data (not reproduced here) indicated that the formula, while adequate in regimes of strong winds, may be unsatisfactory in light winds and highly stable stratifications.

SHEPPARD's formula for the transfer of water vapor may be written

$$F_w = \frac{\varrho k C^{1/2}}{\log\,(k u_* a/\delta)}\, V_a\,(s_s - s_a) \tag{3}$$

SWINBANK (1959) combining observations made by SHEPPARD (1958), and MARCIANO and HARBECK (1952), found that the following gave reasonable results

$$F_L = 5.28 \times 10^{-3}\, V_a\,(e_s - e_a) \text{ cal cm}^{-2} \text{ min}^{-1} \tag{4}$$

Here, F_w has been converted into the equivalent amount of latent heat; V is expressed in m sec^{-1}, and e in millibars.

2. Radiative Fluxes. The radiative transfer of heat was evaluated from radio soundings and observations at sea level, using the radiation chart developed by ELSASSER (1942).

3. Dissipation of Kinetic Energy. This was evaluated from the well-known expression

$$\mathscr{F} = \varrho C V_a^{\,3} + \int_0^\infty \mu \left(\frac{\partial \boldsymbol{v}}{\partial z}\right)^2 dz \tag{5}$$

Since the interest primarily was centered on strong-wind regimes a drag coefficient of 2.6×10^{-3} was used. This value is consistent with the constants of the working formulas (2) and (4).

To the writers' knowledge no accurate determination of μ has been made. It is known (LETTAU, 1951) that μ varies with the stability, but this variation is opposite to that of the shear, with the result that the dissipation within the air column is less variable than μ. In the present computations a standard value of $\mu = 100$ gm cm^{-1} sec^{-1} has been used. This value, which was used by PALMÉN (1959), is somewhat larger than those used by MILDNER (1932), ROSSBY (1935), and others. However, since the internal dissipation is much smaller than the loss at the interface, and since both are small as compared with the supply of sensible heat, the uncertainty in the value of μ is of little consequence.

LIST OF SYMBOLS

A_T	thickness advection (i.e., $-\boldsymbol{v} \cdot \nabla \mathcal{Z}_T$)
A_Q	vorticity advection (i.e., $-\boldsymbol{v} \cdot \nabla Q$)
C	drag coefficient
c_p	specific heat of air at constant pressure
e_a	water vapor pressure of air
e_s	saturation vapor pressure corresponding to T_s
$\mathscr{F}$	frictional dissipation of kinetic energy
F_L	flux of latent heat
F_S	flux of sensible heat
F_W	flux of water vapor
f	Coriolis parameter
g	acceleration of gravity
H	heat received by a unit mass per unit time
k	von Karman's constant
L	latent heat of vaporation
p	pressure
Q	vertical component of absolute vorticity
s	specific humidity
T	temperature
T_a	air temperature
T_s	sea surface temperature
t	time
u_*	friction velocity
$\boldsymbol{v}$	wind vector
V	wind speed
$\mathcal{Z}$	height of isobaric surface
z	vertical coordinate
α	specific volume
δ	molecular diffusivity of water vapor in air (0.25 cm^2 sec^{-1})
θ	potential temperature
$\varkappa$	molecular diffusivity of heat for air (0.21 cm^2 sec^{-1})
q	vertical component of relative vorticity
r	mixing ratio
R	specific gas constant
ϱ	density
σ	a measure of the static stability (i.e., $-\alpha\theta^{-1}\,\partial\theta/\partial p$)
ω	vertical velocity expressed in terms of pressure (i.e., dp/dt)
∇	the two-dimensional differential operator
∇^2	the two-dimensional Laplacian operator

REFERENCES

BJERKNES, J., 1918: On the structure of moving cyclones. *Geofys. Publ.*, Norske Videnskaps-Akademi, Oslo, **1**, 8 pp.

BJERKNES, J., and H. SOLBERG, 1922: Life cycle of cyclones and the polar front theory of atmospheric circulation. *Geofys. Publ.*, Norske Videnskaps-Akademi, Oslo, **3**, 18 pp.

BJERKNES, V., 1921: On the dynamics of the circular vortex with applications to the atmospheric vortex and wave motions. *Geofys. Publ.*, Norske Videnskaps-Akademi, Oslo, **2**, 88 pp.

BURKE, C. J., 1945: Transformation of polar continental air to polar maritime air. *J. Meteor.*, **2**, pp. 94–112.

ELSASSER, W. M., 1942: Heat transfer by infrared radiation in the atmosphere. *Harvard Meteor. Stud.*, No. 6.

ESTOQUE, M. A., 1957: Graphical integration of a two-level model. *J. Meteor.* **14**, 38–42.

HAGE, K. D., 1957: On summer cyclogenesis in western Canada associated with upper cold lows. *Sci. Report* No. 2 under Contract No. AF 19(604)–2179, The University of Chicago.

— 1961: On summer cyclogenesis in the lee of the Rocky Mountains. *Bull. Amer. Meteor. Soc.*, **42**, 21–23.

JACOBS, W. C., 1942: On the energy exchange between sea and atmosphere. *J. Marine Res.*, **5**, 37–66.

LETTAU, H., 1951: Diffusion in the upper atmosphere. *Compendium Meteor.*, Amer. Meteor. Soc., Boston, 320–333.

MARCIANO, J. J. and G. E. HARBECK, 1952: Mass transfer studies. U. S. Dept. Inter. Geol. Surv. No. 229. *Water loss investigations*, Vol. 1. Lake Hefner studies. Tech. Report.

MILDNER, P., 1932: Über die Reibung einer speziellen Luftmasse in dem untersten Schichte der Atmosphäre. *Beitr. Phys. fr. Atm.*, **19**, 151–158.

PALMÉN, E., 1959: On the maintenance of kinetic energy in the atmosphere. *The Atmosphere and Sea in Motion.* The Rockefeller Institute Press and Oxford University Press, New York, 212–223.

PEDERSEN, K., 1961: On the vertical circulation produced by release of latent heat in a static and quasi-geostrophic atmosphere. *Sci. Rep.* No. 5, Contract No. AF 19(604)–7230, The University of Chicago.

PETTERSSEN, S., 1950: Some aspects of the general circulation of the atmosphere. *Cent. Proc. Roy. Meteor. Soc.*, London, 120–155.

— 1955: A general survey of factors influencing development at sea level. *J. Meteor.*, **12**, 34–42.

— 1956: *Weather Analysis and Forecasting*, Vol. 1. McGraw-Hill Book Co., New York.

PETTERSSEN, S., and P. A. CALABRESE, 1959: On some weather influences due to warming of the air by the Great Lakes in winter. *J. Meteor.* **16**, 646–652.

PETTERSSEN, S., G. E. DUNN and L. L. MEANS, 1955: Report of an experiment in forecasting of cyclone development. *J. Meteor.*, **12**, 58–67.

PRIESTLEY, C. H. B., and W. C. SWINBANK, 1947: Vertical transport of heat by turbulence in the atmosphere. *Proc. Roy. Soc.* **A 189**, 543–561.

ROSSBY, C.-G., and R. B. MONTGOMERY, 1935: The layer of frictional influence in wind and ocean currents. *Papers in Phys. Oceanogr. and Met.*, **3**, No. 3.

SAWYER, J. S., and F. H. BUSHBY, 1953: A baroclinic model atmosphere suitable for numerical integration. *J. Meteor.* **10**, 54–59.

SHEPPARD, P. A., 1958: Transfer across the earth's surface and through the air above. *Quart. J. R. Met. Soc.* **84**, 205–224.

SMEBYE, S. J., 1958: Computations of precipitation from large-scale vertical motion. *J. Meteor.* **15**, 547–560.

SWINBANK, W. C., 1959: Evaporation from the oceans. *Sci. Rep.* No. 12, Contract No. AF 19 (604) –2179, The University of Chicago.

(Manuscript received December 18, 1961)